Chapter 3

A Modified Current Injection Load Flow Method Under Different Load Model of EV for Distribution System

3.1 Introduction

The last chapter addresses the generation of stochastic modelling of PHEV load on distribution system with consideration of uncertainties related to driving behaviour of vehicles. This chapter presents a modified method of reliable and robust power flow algorithm with inclusion of different EV load models in context of planning and operation of distribution system.

The charging load demand and load characteristics of EVs are correlated to the charging scenario, and hence, it influences the EV load modelling i.e, EVs load can be modelled as PV bus as well as PQ bus in load flow studies. Thus, it is essential to examine the affect of EV load model taking into account the effect of grid voltage and state of charge (SOC) of EVs by reliable and robust power flow method for planning and operation of the existing distribution systems. In existing literature, the process for the adoption of the existing EV load model is done with the application of Newton-Raphson load-flow algorithm to examine the effect of EV on distribution systems.

Conventional power flow analysis based on Newton-Raphson has limitation of convergence when applied to the distribution system with large number of PV buses. The Current Injection-based Newton-Raphson (CINR) load flow algorithm has the ability to

circumvent the problem of convergence and handling of PV buses in radial distribution system.

In this chapter, the modified current injection based power flow analysis ($MCINR$) of modern distribution network (having large number of PV buses) with inclusion of three different types of EV load models is proposed. In the proposed formulation, a modification in the representation of PV buses according to the considered EV load model is presented. In addition to this, the effectiveness and the efficiency of proposed modified current injection load flow algorithm are also verified in terms of convergence characteristics with different EV load model on 38-bus distribution system. The proposed method is also tested on both the unbalanced radial system (18-, 84- and 140-bus) and meshed distribution test systems (24-, 118- and 300-bus). For performance assessment, performance of proposed load flow algorithm ($MCINR$) is also compared with existing load flow algorithms ($CINR-1$, $CINR-2$ and CNR) in terms of convergence speed with varying load profiles and R/X ratios of lines. Moreover, the proposed load flow algorithm is implemented to evaluate the system performance indices to examine the effects of different EV load modelling in the 38-bus distribution system. Three impact indices are considered in this work, aiming to measure effects of different EV load models on modern distribution system planning and operation. The indices including: real power loss index (ILP), reactive power loss index (ILQ), voltage profile index (IVD) and MVA capacity index (IC) are obtained using numerical simulation carried out on the 38-bus distribution system in presence of DGs.

3.2 Load Modelling

3.2.1 EV load modelling

Evaluation of effect of EV load modeling for distribution system planning studies requires a detailed characteristics of battery and charging technology. The charging load demand and load characteristics of EVs are correlated to the charging scenario, and hence, it influences the load modelling. All the three types of EV load models considered in this work are described as follows.

EV Load Model-I ($EVLM$-I)

The first type of EV load model is a polynomial type or ZIP ($EVLM$-I) load model. The real and reactive load of EV in the distribution system depends on the voltage of buses and can be represented by the polynomial equations (3.1) and (3.2) respectively.

$$P_{EVLM-I} = P_{0k}\{\alpha_p + \beta_p V_k + \gamma_p V_k^2\}, \tag{3.1}$$

$$Q_{EVLM-I} = Q_{0k}\{\alpha_q + \beta_q V_k + \gamma_q V_k^2\}, \tag{3.2}$$

where, P_{EVLM-I} and Q_{EVLM-I} are total required active and reactive powers respectively while considering $EVLM-I$ load model.

The parameters of ZIP model used in the present work are taken from [66]. The ZIP model obtained in [66] is based on experimental measurements made in the SOC range of 10-100% at different voltage levels. The authors of ref. [66] have used a constrained least square method to determine the ZIP coefficients of the models given in equation (3.1) and (3.2). Table 3.1 gives the best fit values, subject to following conditions.

$$\alpha_p + \beta_p + \gamma_p = 1,$$

and

$$\alpha_q + \beta_q + \gamma_q = 1.$$

Table 3.1: ZIP Parameters for $EVLM-I$

	α_p	β_p	γ_p	α_q	β_q	γ_q
$EVLM-I$	-0.1773	0.9949	0.1824	4.993	-12.910	8.917

EV Load Model-II ($EVLM$-II)

The second type of load model ($EVLM$-II) is a voltage-dependent load model. For voltage stability studies, energy required by charger should be monitored during fluctuations in system voltages. For this work, derived voltage dependent load model of EV charger is adopted from [69,157]. Mathematically, active power of EV can be represented as follows.

$$P_{EVLM-II} = P_{0k}\{\alpha_p + \beta_p V_k^a\}, \tag{3.3}$$

where, $P_{EVLM-II}$ is total required active power while considering $EVLM-II$ load model.

The first term of equation (3.3) represents constant power part and second term represents voltage-dependent part of the load. The voltage dependent load model parameters, α_p, β_p and a are 0.9279, 0.0721 and -3.101 respectively [69]. The reactive power is calculated using the active power and the power factor ($cos\theta$) of the charger. The reactive power is calculated using the following relation.

$$Q_{EVLM-II} = P_{EVLM-II} \tan\theta,$$

$$Q_{EVLM-II} = P_{0k}\{\alpha_p + \beta_p V_k^a\} \tan\theta, \tag{3.4}$$

where, $Q_{EVLM-II}$ is total required reactive power while considering $EVLM-II$ load model. In this work, value of power factor ($cos\theta$) is taken as 0.97.

EV Load Model-III ($EVLM$-III)

The third type of load model ($EVLM$-III) is constant current load model [70]. In this model, active power is described using the following relation.

$$P_{EVLM-III} = P_{0k} V_k^{\alpha_{EV}}.$$

For electric vehicle chargers, α_{EV} is assumed to be 1. Thus, above equation can be written as,

$$P_{EVLM-III} = P_{0k} V_k, \tag{3.5}$$

and,

$$Q_{EVLM-III} = 0. \tag{3.6}$$

Here, $P_{EVLM-III}$ is total required active power while considering $EVLM-III$ load model. It is to be noted that in this model the reactive power taken by EV, $Q_{EVLM-III}$, is assumed to be zero.

3.2.2 Conventional load modelling

Power system loads normally comprises of residential, industrial and commercial loads. These loads are sensitive to variation in the voltage and frequency [71]. The static polynomial load model or ZIP model demonstrates the effect of voltage in power-voltage equation and this consists of three static load models viz. constant impedance (CI), constant current (CC) and constant power (CP) load models. Power-voltage relationship

equation of the load can be expressed as follows.

$$P_k = P_{0k}\{\alpha_p + \beta_p V_k + \gamma_p V_k^2\}.$$

Similarly, reactive power of the load can be modelled as,

$$Q_k = Q_{0k}\{\alpha_q + \beta_q V_k + \gamma_q V_k^2\}.$$

A survey based on customer class was performed in order to produce the polynomial load model of residential, commercial and industrial loads [60]. In the present study, a specific class of residential customer (stratum D), large commercial and industrial customers are considered and the corresponding ZIP coefficient parameters values given in [60] are used in this study and are given in Table 3.2.

Table 3.2: ZIP Parameters of conventional load

Customer Class	α_p	β_p	γ_p	α_q	β_q	γ_q
Residential	1.63	-1.94	1.31	7.07	-15.27	9.2
Commercial	0.76	-0.52	0.76	5.83	-11.75	6.92
Industrial	1.41	-1.61	1.21	3.72	-7.08	4.35

3.3 Problem Formulation

In this section, the modified current injection Newton-Raphson ($MCINR$) based load flow formulation considering different EV load models and handling of PQ and PV-buses for the distribution systems is described. In order to present the modifications in the existing $CINR$ method [79], power flow formulation is expressed in rectangular coordinates as presented in next subsection.

3.3.1 Power flow equations

The active and reactive current mismatch at k^{th}-bus is given by,

$$\Delta I_{rk} = \sum_{i=1}^{n}(G_{ki}V_{ri} - B_{ki}V_{mi}) - \frac{P_k V_{rk} + Q_k V_{mk}}{(V_{rk})^2 + (V_{mk})^2} \tag{3.7}$$

and,

$$\Delta I_{mk} = \sum_{i=1}^{n}(B_{ki}V_{ri} + G_{ki}V_{mi}) - \frac{P_k V_{mk} - Q_k V_{rk}}{(V_{rk})^2 + (V_{mk})^2}. \tag{3.8}$$

Taylor's series expansion of equations (3.7) and (3.8) after neglecting the higher order terms, gives the following equation,

$$\begin{bmatrix} \Delta I_{rk} \\ \Delta I_{mk} \end{bmatrix} = \sum_{\substack{i=1,\\ i\neq k}}^{n} \begin{bmatrix} G_{ki} & -B_{ki} \\ B_{ki} & G_{ki} \end{bmatrix} \begin{bmatrix} \Delta V_{ri} \\ \Delta V_{mi} \end{bmatrix} + \begin{bmatrix} G'_{kk} & B'_{kk} \\ B''_{kk} & G''_{kk} \end{bmatrix} \begin{bmatrix} \Delta V_{rk} \\ \Delta V_{mk} \end{bmatrix} - \frac{1}{V_k^2} \begin{bmatrix} V_{rk} & V_{mk} \\ V_{mk} & -V_{rk} \end{bmatrix} \begin{bmatrix} \Delta P_k \\ \Delta Q_k \end{bmatrix}. \tag{3.9}$$

Here, values of G'_{kk}, B'_{kk}, G''_{kk} and B''_{kk} are dependent on the type of the k^{th}-bus in the distribution system.

3.3.2 Representation of PQ buses for different EV load model

In case of the PQ buses, injected real power (P_k) and reactive power (Q_k) are specified in the power flow problem, where, 'k' is assumed as a PQ bus in the distribution system.

EV Load Model-I ($EVLM$-I)

Total injected active and reactive powers at the k^{th}-bus can be calculated using following equations,

$$P_k = P_{gk} - P_{EVLM-Ik}, \tag{3.10}$$

$$Q_k = Q_{gk} - Q_{EVLM-Ik}. \tag{3.11}$$

Linearised equations corresponding to equations (3.10) and (3.11) can be expressed as follows,

$$\Delta P_k = \Delta P_{gk} - \Delta P_{EVLM-Ik}, \tag{3.12}$$

$$\Delta Q_k = \Delta Q_{gk} - \Delta Q_{EVLM-Ik}. \tag{3.13}$$

Here, $\Delta P_{EVLM-Ik}$, $\Delta Q_{EVLM-Ik}$ are total required active and reactive power mismatches respectively while considering $EVLM-I$ at k^{th} bus.

Considering above linearizations and, taking $\Delta P_{gk} = 0$ and $\Delta Q_{gk} = 0$ at PQ buses, equations (3.1) and (3.2) become,

$$\Delta P_{EVLM-Ik} = -P_{0k} \left(\beta_p + 2V_k\gamma_p\right) \Delta V_k \tag{3.14}$$

$$\Delta Q_{EVLM-Ik} = -Q_{0k} \left(\beta_q + 2V_k\gamma_q\right) \Delta V_k \tag{3.15}$$

Linearised equations (3.14) and (3.15) corresponding to equations (3.12) and (3.13) can be expressed as follows.

$$\Delta P_k = -P_{0k} \left(\beta_p + 2V_k\gamma_p\right) \Delta V_k, \tag{3.16}$$

$$\Delta Q_k = -Q_{0k}\left(\beta_q + 2V_k\gamma_q\right)\Delta V_k. \tag{3.17}$$

EV Load Model-II ($EVLM$-II)

Linearised equations corresponding to real and reactive powers injected at bus k can be given by the following relations,

$$\Delta P_k = \Delta P_{gk} - \Delta P_{EVLM-IIk}, \tag{3.18}$$

and

$$\Delta Q_k = \Delta Q_{gk} - \Delta Q_{EVLM-IIk}. \tag{3.19}$$

Here, $\Delta P_{EVLM-IIk}$ and $\Delta Q_{EVLM-IIk}$ are total required active and reactive power mismatches respectively while considering $EVLM-II$ at k^{th} bus.

Considering above linearizations and, taking $\Delta P_{gk} = 0$ and $\Delta Q_{gk} = 0$ at PQ buses, equations (3.3) and (3.4) become,

$$\Delta P_{EVLM-IIk} = -P_{0k}\beta_p a V_k^{a-1}\Delta V_k \tag{3.20}$$

$$\Delta Q_{EVLM-IIk} = -P_{0k}\tan\theta\beta_p a V_k^{a-1}\Delta V_k \tag{3.21}$$

Linearised equations (3.20) and (3.21) corresponding to equations (3.18) and (3.19) can be expressed as follows.

$$\Delta P_k = -P_{0k}\beta_p a V_k^{a-1}\Delta V_k, \tag{3.22}$$

$$\Delta Q_k = -P_{0k}\tan\theta\beta_p a V_k^{a-1}\Delta V_k. \tag{3.23}$$

EV Load Model-III ($EVLM$-III)

Linearised equations corresponding to real and reactive powers injected at k^{th} bus are given by,

$$\Delta P_k = \Delta P_{gk} - \Delta P_{EVLM-IIIk}, \tag{3.24}$$

and

$$\Delta Q_k = \Delta Q_{gk} - \Delta Q_{EVLM-IIIk}. \tag{3.25}$$

Here, $\Delta P_{EVLM-IIIk}$ and $\Delta Q_{EVLM-IIIk}$ are total required active and reactive power mismatches respectively while considering $EVLM-III$ load model at k^{th} bus.

Considering above linearizations and, taking $\Delta P_{gk} = 0$ and $\Delta Q_{gk} = 0$ at PQ buses, equations (3.5) and (3.6) become,

$$\Delta P_{EVLM-IIIk} = P_{0k}\Delta V_k \tag{3.26}$$

$$\Delta Q_{EVLM-IIIk} = 0 \tag{3.27}$$

Linearised equations (3.26) and (3.27) corresponding to equations (3.24) and (3.25) can be expressed as follows.

$$\Delta P_k = P_{0k}\Delta V_k, \tag{3.28}$$

Similarly,

$$\Delta Q_k = 0, \tag{3.29}$$

and,

$$\Delta V_k = \frac{1}{V_k}\left(V_{rk}\Delta V_{rk} + V_{mk}\Delta V_{mk}\right). \tag{3.30}$$

Using the values of ΔP_k, ΔQ_k from load models of $EVLM\text{-}I$, $EVLM\text{-}II$ and $EVLM\text{-}III$ and ΔV_k from equation (3.30), equation (3.9) become.

$$\begin{bmatrix}\Delta I_{rk}\\ \Delta I_{mk}\end{bmatrix} = \sum_{\substack{i=1,\\ i\neq k}}^{n}\begin{bmatrix}G_{ki} & -B_{ki}\\ B_{ki} & G_{ki}\end{bmatrix}\begin{bmatrix}\Delta V_{ri}\\ \Delta V_{mi}\end{bmatrix} + \begin{bmatrix}A & B\\ C & D\end{bmatrix}\begin{bmatrix}\Delta V_{rk}\\ \Delta V_{mk}\end{bmatrix}, \tag{3.31}$$

where, A, B, C and D for EV load model $EVLM\text{-}I$, $EVLM\text{-}II$ and $EVLM\text{-}III$ are evaluated using following equations.

- A, B, C and D for EV load model $EVLM\text{-}I$:-

$$\begin{aligned}A =& G_{kk} - \frac{1}{V_k^4}\Big(V_{mk}^2\{P_{gk} - P_{0k}(\alpha_p + \beta_p V_k + \gamma_p V_k^2)\} - V_{rk}^2\{P_{gk} - P_{0k}(\alpha_p - \gamma_p V_k^2)\}\\ &- V_{rk}V_{mk}\{2Q_{gk} - Q_{0k}(2\alpha_q + \beta_q V_k)\}\Big)\\ B =& -B_{kk} - \frac{1}{V_k^4}\Big(V_{rk}^2\{Q_{gk} - Q_{0k}(\alpha_q + \beta_q V_k + \gamma_q V_k^2)\} - V_{mk}^2\{Q_{gk} - Q_{0k}(\alpha_q - \gamma_q V_k^2)\}\\ &- V_{rk}V_{mk}\{2P_{gk} - P_{0k}(2\alpha_p + \beta_p V_k)\}\Big)\\ C =& B_{kk} - \frac{1}{V_k^4}\Big(V_{rk}^2\{Q_{gk} - Q_{0k}(\alpha_q - \gamma_q V_k^2)\} - V_{mk}^2\{Q_{gk} - Q_{0k}(\alpha_q + \beta_p V_k + \gamma_p V_k^2)\}\\ &- V_{rk}V_{mk}\{2P_{gk} - P_{0k}(2\alpha_p + \beta_p V_k)\}\Big)\\ D =& G_{kk} + \frac{1}{V_k^4}\Big(V_{mk}^2\{P_{gk} - P_{0k}(\alpha_p - \gamma_p V_k^2)\} - V_{rk}^2\{P_{gk} - P_{0k}(\alpha_p + \beta_p V_k + \gamma_p V_k^2)\}\\ &- V_{rk}V_{mk}\{2Q_{gk} - Q_{0k}(2\alpha_q + \beta_q V_k)\}\Big)\end{aligned}$$

- A, B, C and D for EV load model $EVLM\text{-}II$:-

$$A = G_{kk} - \frac{1}{V_k^4}\Big(V_{mk}^2\{P_{gk} - P_{0k}(\alpha_p + \beta_p V_k^a)\} - V_{rk}^2\{P_{gk} - P_{0k}(\alpha_p + \beta_p(1-a)V_k^a)\} - V_{rk}V_{mk}\{2Q_{gk} - P_{0k}\tan\theta(2\alpha_p + \beta_p(2-a)V_k^a)\}\Big)$$

$$B = -B_{kk} - \frac{1}{V_k^4}\Big(V_{rk}^2\{Q_{gk} - P_{0k}\tan\theta(\alpha_p + \beta_p V_k^a)\} - V_{mk}^2\{Q_{gk} - P_{0k}\tan\theta(\alpha_p + \beta_p (2-a)V_k^a)\} - V_{rk}V_{mk}\{2P_{gk} - P_{0k}\tan\theta(2\alpha_p + \beta_p(2-a)V_k^a)\}\Big)$$

$$C = B_{kk} - \frac{1}{V_k^4}\Big(V_{rk}^2\{Q_{gk} - P_{0k}\tan\theta(\alpha_p + \beta_p(1+a)V_k^a)\} - V_{mk}^2\{Q_{gk} - P_{0k}\tan\theta(\alpha_p + \beta_p V_k^a)\} - V_{rk}V_{mk}\{2P_{gk} - P_{0k}\tan\theta(2\alpha_p + \beta_p(2-a)V_k^a)\}\Big)$$

$$D = G_{kk} + \frac{1}{V_k^4}\Big(V_{mk}^2\{P_{gk} - P_{0k}(\alpha_p + \beta_p(1+a)V_k^a)\} - V_{rk}^2\{P_{gk} - P_{0k}(\alpha_p + \beta_p V_k^a)\} - V_{rk}V_{mk}\{2Q_{gk} - P_{0k}\tan\theta(2\alpha_p + \beta_p(2-a)V_k^a)\}\Big)$$

- A, B, C and D for EV load model $EVLM\text{-}III$:-

$$A = G_{kk} - \frac{1}{V_k^4}\Big(V_{mk}^2\{P_{gk} - P_{0k}V_k\} - V_{rk}^2\{P_{gk} - P_{0k}V_k\} - 2V_{rk}V_{mk}Q_{gk}\Big)$$

$$B = -B_{kk} - \frac{1}{V_k^4}\Big(V_{rk}^2 Q_{gk} - V_{mk}^2 Q_{gk}V_k - V_{rk}V_{mk}(P_{gk} - 3P_{0k}V_k)\Big)$$

$$C = B_{kk} - \frac{1}{V_k^4}\Big(V_{rk}^2 Q_{gk} - V_{mk}^2 Q_{gk}V_k - V_{rk}V_{mk}(P_{gk} - 3P_{0k}V_k)\Big)$$

$$D = G_{kk} + \frac{1}{V_k^4}\Big(V_{mk}^2\{P_{gk} - 2P_{0k}V_k\} - V_{rk}^2\{P_{gk} - P_{0k}V_k\} - 2V_{rk}V_{mk}Q_{gk}\Big)$$

3.3.3 Representation of PV buses

In case of PV buses, reactive power, (Q_k), of the PV bus is not specified. Q_k for a PV bus can be can be calculated as follows,

$$Q_k = V_{mk}I_{rk}^{cal} - V_{rk}I_{mk}^{cal}.$$

As $\Delta P_{gk} = 0$ and $\Delta V_k = 0$ at PV buses, the equations for the ΔP_k and ΔQ_k for $EVLM\text{-}I$, $EVLM\text{-}II$ and $EVLM\text{-}III$ become,

$$\Delta P_k = \Delta P_g = 0,$$

and

$$\Delta Q_k = \Delta Q_{gk},$$

and from equation (3.30),

$$\Delta V_{rk} = -\frac{V_{mk}}{V_{rk}} \Delta V_{mk}.$$

After substituting the values of ΔQ_k and ΔV_{rk} equation (3.9) becomes,

$$\begin{bmatrix} \Delta I_{rk} \\ \Delta I_{mk} \end{bmatrix} = \sum_{\substack{i=1, \\ i \neq k}}^{n} \begin{bmatrix} G_{ki} & -B_{ki} \\ B_{ki} & G_{ki} \end{bmatrix} \begin{bmatrix} \Delta V_{ri} \\ \Delta V_{mi} \end{bmatrix} + \begin{bmatrix} G_{kk}^{'} & B_{kk}^{'} \\ B_{kk}^{"} & G_{kk}^{"} \end{bmatrix} \begin{bmatrix} -\frac{V_{mk}}{V_{rk}} \Delta V_{mk} \\ \Delta V_{mk} \end{bmatrix} - \frac{1}{V_k^2} \begin{bmatrix} V_{rk} & V_{mk} \\ V_{mk} & -V_{rk} \end{bmatrix} \begin{bmatrix} 0 \\ \Delta Q_g \end{bmatrix}, \tag{3.32}$$

where,

$$G_{kk}^{'} = G_{kk} - \frac{1}{V_k^4}(V_{mk}^2\{P_k - 2V_{rk}I_{rk}^{cal}\} - V_{rk}^2\{P_k + 2V_{mk}I_{mk}^{cal}\}),$$

$$B_{kk}^{'} = -B_{kk} - \frac{1}{V_k^4}(V_{mk}\{(V_{rk}^2 - V_{mk}^2)I_{rk}^{cal} - V_{rk}P_k\} - V_{rk}\{(V_{rk}^2 - V_{mk}^2)I_{mk}^{cal} - V_{mk}P_k\}),$$

$$B_{kk}^{''} = B_{kk} - \frac{1}{V_k^4}(V_{mk}\{(V_{rk}^2 - V_{mk}^2)I_{rk}^{cal} - V_{rk}P_k\} - V_{rk}\{(V_{rk}^2 - V_{mk}^2)I_{mk}^{cal} - V_{mk}P_k\}),$$

$$G_{kk}^{''} = G_{kk} + \frac{1}{V_k^4}(V_{mk}^2(P_k - 2V_{rk}I_{rk}^{cal}) - V_{rk}^2(P_k + 2V_{mk}I_{mk}^{cal})).$$

Upon simplification equation (3.32) becomes,

$$\begin{bmatrix} \Delta I_{rk} \\ \Delta I_{mk} \end{bmatrix} = \sum_{\substack{i=1, \\ i \neq k}}^{n} \begin{bmatrix} G_{ki} & -B_{ki} \\ B_{ki} & G_{ki} \end{bmatrix} \begin{bmatrix} \Delta V_{ri} \\ \Delta V_{mi} \end{bmatrix} + \begin{bmatrix} B_{kk}^{'} - \frac{V_{mk}}{V_{rk}} G_{kk}^{'} & -\frac{V_{mk}}{V_k^2} \\ B_{kk}^{"} - \frac{V_{mk}}{V_{rk}} G_{kk}^{"} & \frac{V_{rk}}{V_k^2} \end{bmatrix} \begin{bmatrix} \Delta V_{mk} \\ \Delta Q_g \end{bmatrix}. \tag{3.33}$$

3.3.4 Jacobian structure

The proposed $MCINR$ algorithm can be written in the compact form as follows.

$$\begin{bmatrix} \Delta I_{rm}^{pq} \\ \cdots \\ \Delta I_{rm}^{pv} \end{bmatrix} = \begin{bmatrix} J_{pq-pq} & J_{pq-pv} \\ J_{pv-pq} & J_{pv-pv} \end{bmatrix} \begin{bmatrix} \Delta V_{rm}^{pq} \\ \cdots \\ \Delta V_{mQ}^{pv} \end{bmatrix},$$

where,

$$\Delta I_{rm}^{pq} = \Big[\Delta I_{r1}, \Delta I_{r2}, \ldots, \Delta I_{rn}, \Delta I_{m1}, \Delta I_{m2}, \ldots, \Delta I_{mn}\Big]^T,$$

$$\Delta I_{rm}^{pv} = \Big[\Delta I_{r(n+1)}, \Delta I_{r(n+2)}, \ldots, \Delta I_{rN}, \Delta I_{m(n+1)}, \Delta I_{m(n+2)}, \ldots, \Delta I_{mN}\Big]^T,$$

$$\Delta V_{rm}^{pq} = \Big[\Delta V_{r1}, \Delta V_{r2}, \ldots, \Delta V_{rn}, \Delta V_{m1}, \Delta V_{m2}, \ldots, \Delta V_{mn}\Big]^T,$$

$$\Delta V_{mQ}^{pv} = \Big[\Delta V_{m(n+1)}, \Delta V_{m(n+2)}, \ldots, \Delta V_{mN}, \Delta Q_{(n+1)}, \Delta Q_{(n+2)}, \ldots, \Delta Q_N\Big]^T,$$

$$J_{pq-pq} = \left[\begin{array}{c|c} \mathbf{G}' & \mathbf{B}' \\ \hline \mathbf{B}'' & \mathbf{G}'' \end{array}\right] \ ,$$

$$J_{pq-pv} = \left[\begin{array}{c|c} -\mathbf{B} - \frac{V_m}{V_r}\mathbf{G} & 0 \\ \hline \mathbf{G} - \frac{V_m}{V_r}\mathbf{B} & 0 \end{array}\right] \ ,$$

$$J_{pv-pv} = \left[\begin{array}{c|c} \mathbf{B}^{*\prime} - \frac{V_m}{V_r}\mathbf{G}^{*\prime} & -\frac{V_m}{V^2} \\ \hline \mathbf{G}^{*\prime\prime} - \frac{V_m}{V_r}\mathbf{B}^{*\prime\prime} & \frac{V_r}{V^2} \end{array}\right] \ ,$$

$$J_{pv-pq} = \left[\begin{array}{c|c} \mathbf{G} & -\mathbf{B} \\ \hline \mathbf{B} & \mathbf{G} \end{array}\right] \text{ and,}$$

$$\begin{bmatrix} \Delta V_{rm}^{pq} \\ \dots \\ \Delta V_{mQ}^{pv} \end{bmatrix} = \begin{bmatrix} J_{pq-pq} & J_{pq-pv} \\ J_{pv-pq} & J_{pv-pv} \end{bmatrix}^{-1} \begin{bmatrix} \Delta I_{rm}^{pq} \\ \dots \\ \Delta I_{rm}^{pv} \end{bmatrix}. \tag{3.34}$$

Equation (3.34) can be generalized as,

$$\Big[\Delta V\Big] = \Big[J\Big]^{-1} \Big[\Delta I\Big].$$

Consequently using above equations voltage update can be written as follows,

$$V^{iter+1} = V^{iter} + \Delta V. \tag{3.35}$$

For the sake of clarity, the solution procedure of $MCINR$ is summarized in the flowchart shown in Fig. 3.1. The step-by-step procedure of $MCINR$ is shown in Algorithm 2.

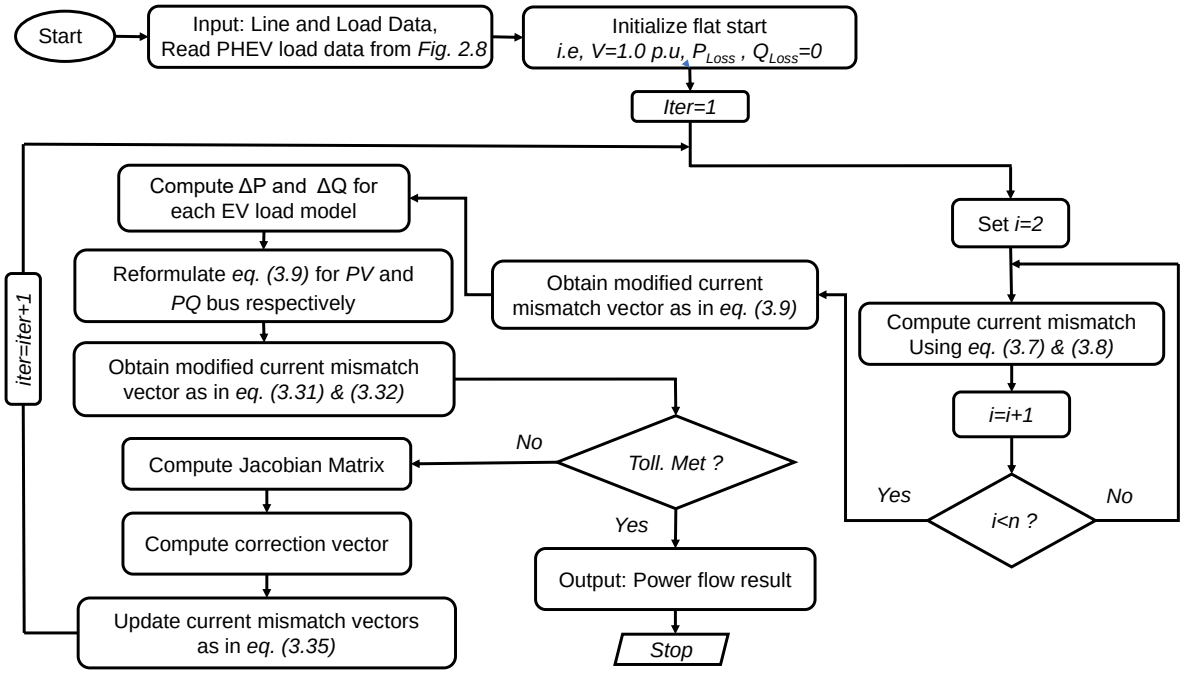

Figure 3.1: Solution procedure of $MCINR$

3.4 Case Study

In this section, impact of different EV load models on the distribution system load flow are carried out to substantiate its effectiveness with different penetration levels of vehicles.

3.4.1 Test system

The 38-bus distribution network, shown in Fig. 3.2 has been taken for study and analysis. The detailed specifications of bus-wise load , line parameters, MVA capacity of the test system and types of customers are listed in Appendix I. The distribution system is energized through CPG which is connected at bus-1. The hourly load distribution of a day is shown in Fig. 3.3. A total of 250 PHEVs and 10 DGs are considered in this study. According to EPRI's technical report, the penetration of EVs in distribution system is expected to increase from 35% in 2020 to 62% in 2050 [5]. Following are the assumptions made in this study.

- PHEVs are equally distributed on the residential buses.
- Charging of PHEVs are done only at the residential buses.

Algorithm 2:

1 Calculate nodal admittance matrix, $Y = G + jB$;

2 Initialize real and imaginary voltage, $V_{rk} = 1$ and $V_{mk} = 0$, $k = 1, .., n$ for PQ Buses, and imaginary voltage $V_{mk} = 0$,for $k = n + 1, ..., N$ for PV Buses.

3 Start the iterative process with h (Iteration number) $= 0$

4 Determine current injection, $I_r^{cal} + jI_m^{cal} = I^{cal} = YE = (G + jB) \times (V_r + jV_m)$.

5 Determine active and reactive power mismatch.

$$\Delta P_k = P_k - (I_r^{cal} V_r + I_m^{cal} V_m),$$

$$\Delta Q_k = Q_k - (I_r^{cal} V_m + I_m^{cal} V_r)$$

.

6 **While** $(max(\Delta P, \Delta Q) \leq Tolerance$ or $h > max)$

7 $h = h + 1$.

8 Calculate the current mismatch

$$\triangle I_{rk} = \frac{V_{rk} \triangle P_k + V_{mk} \triangle Q_k}{V_k^2},$$

$$\triangle I_{mk} = \frac{V_{mk} \triangle P_k - V_{rk} \triangle Q_k}{V_k^2}$$

9 Calculate Jacobian Matrix.

10 Determine the correction in bus voltages

11 Update the bus voltage

$$V_{rk}^{h+1} = V_{rk}^h + \Delta V_{rk}^h$$

$$V_{mk}^{h+1} = V_{mk}^h + \Delta V_{mk}^h$$

12 Current injection,$I_r^{cal} + jI_m^{cal} = I^{cal} = YE = (G + jB) \times (V_r + jV_m)$.

13 Active and reactive power mismatch

$$\Delta P_k = P_k - (I_r^{cal} V_r + I_m^{cal} V_m)$$

$$\Delta Q_k = Q_k - (I_r^{cal} V_m + I_m^{cal} V_r)$$

Endwhile

14 Print result

- All the residential buses are well equipped with smart metering system to calculate the energy for G2V and V2G operation.

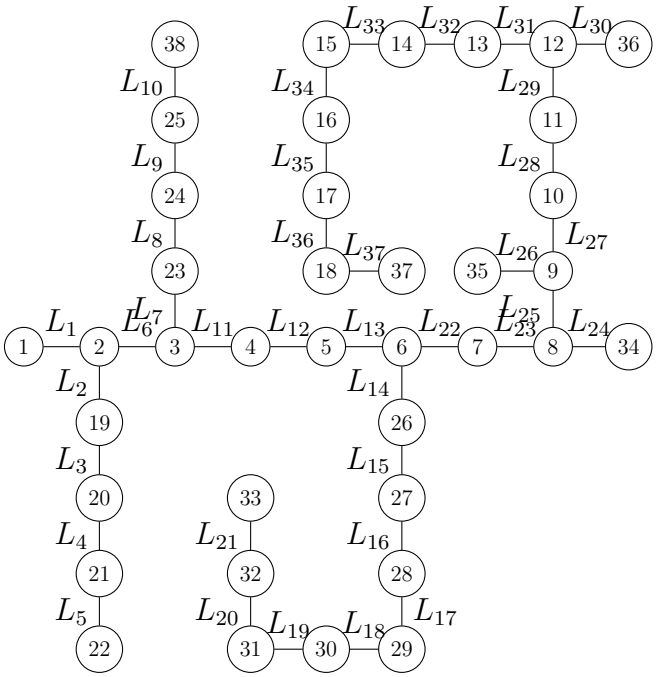

Figure 3.2: The 38-bus distribution system

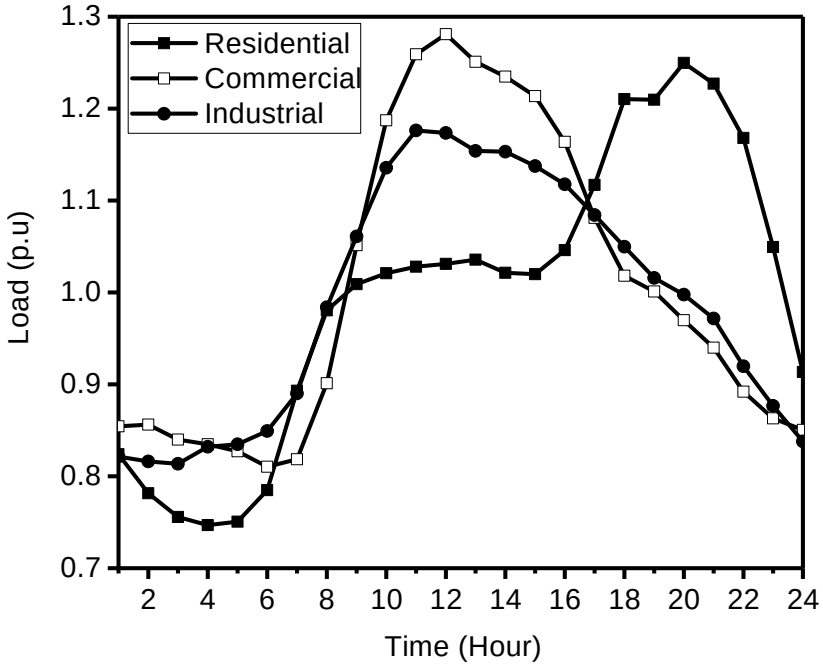

Figure 3.3: Average load demand

The detailed characteristics of DGs including the type of DGs and the hourly availability are given in Appendix II. Candidate buses for the DGs placement are determined on the basis of minimization of energy losses in the system. These locations will be the input to the system model. The selection of candidate buses has been performed for all dispatchable DGs in 38-bus system for all the load models using a Mixed Integer Non-Linear Programming (MINLP) approach as given in Appendix III .

3.4.2 EV load model impact indices

In this work, following indices will be computed in order to describe the effect of inclusion of EV load models in load flow programs in presence of DGs.

Real and reactive power loss indices (ILP & ILQ)

The real and reactive power loss indices are defined as follows.

$$ILP = \frac{P_{DLG}}{P_L},$$

$$ILQ = \frac{Q_{DLG}}{Q_L},$$

where, P_{DLG} and Q_{DLG} are the active and reactive power losses respectively in the presence of DGs. P_L and Q_L are the active and reactive power losses respectively in the absence of DGs.

Voltage profile index (IVD)

The Voltage profile index (IVD) gives voltage deviation from the nominal values ($V_1 = 1.03$).

Expression for IVD is as follows.

$$IVD = max_{i=2}^{n}\left\{\frac{|V_1| - |V_i|}{|V_1|}\right\}.$$

The value of IVD should be monitored to keep it within allowable limits for assuring power quality. Therefore it is needed to evaluate the influence of load model on system voltage profile.

MVA Capacity Index (IC)

For the DERs near loads, it is quite probable that MVA flow may reduce in some sections, thus releasing more capacity, whereas in other sections MVA flow may increases surpassing distribution line limits.

Index IC provides a information regarding the level of MVA flows across line concerning maximum capacity of conductors analogous to that line. System line up-gradation is accomplished based on this information. If values of IC is more than unity it indicates capacity violation in terms of line flows. Lower value of IC indicates availability of MVA capacity of line.

MVA capacity index (IC) can be calculated as follows.

$$IC = max_{i=1}^{n} \frac{|\overline{S_{ij}}|}{|\overline{CS_{ij}}|}.$$

where, $\overline{S_{ij}}$ is MVA flow in the line connecting the buses i and j (i.e line $i-j$) and $\overline{CS_{ij}}$ is MVA capacity of line i-j .

3.4.3 Performance assessment of $MCINR$

In this section, the convergence characteristics in terms of the number of iterations required to converge to the tolerance limit of $CINR-I$, $CINR-II$ and $MCINR$ are compared for all the three EV load models. In addition to this, to validate efficacy and robustness of proposed load flow algorithm $MCINR$, it is also tested on the unbalanced radial system (18-, 84- and 140-bus) and meshed distribution test systems (24-, 118- and 300-bus).

The tolerance limit of 10^{-8} is used as a stopping criterion for all the algorithms. The maximum number of iterations for all the algorithm has been fixed to 15.

Convergence characteristics of MCINR with different EV load model

Maximum power mismatch $max(\Delta P)$ of $CINR-I$, $CINR-II$ and $MCINR$ on each iteration for EV load models $EVLM$-I, $EVLM$-II and $EVLM$-III are shown in Figs. 3.4, 3.5 and 3.6 . It is observed that the convergence characteristic in terms of maximum power mismatch is better in case of modified current injection Newton-Raphson ($MCINR$) as compared to $CINR-I$, $CINR-II$. At this point, it is also important to

note from the results, that the convergence rate is faster with all three EV Load models and required number of iterations is lesser for $EVLM-II$ and $EVLM-III$. Whereas, with constant current load model ($EVLM-III$), required number of iterations is same for all existing current injection-based power flow viz. $CINR-I$ and $CINR-II$ and the proposed $MCINR$.

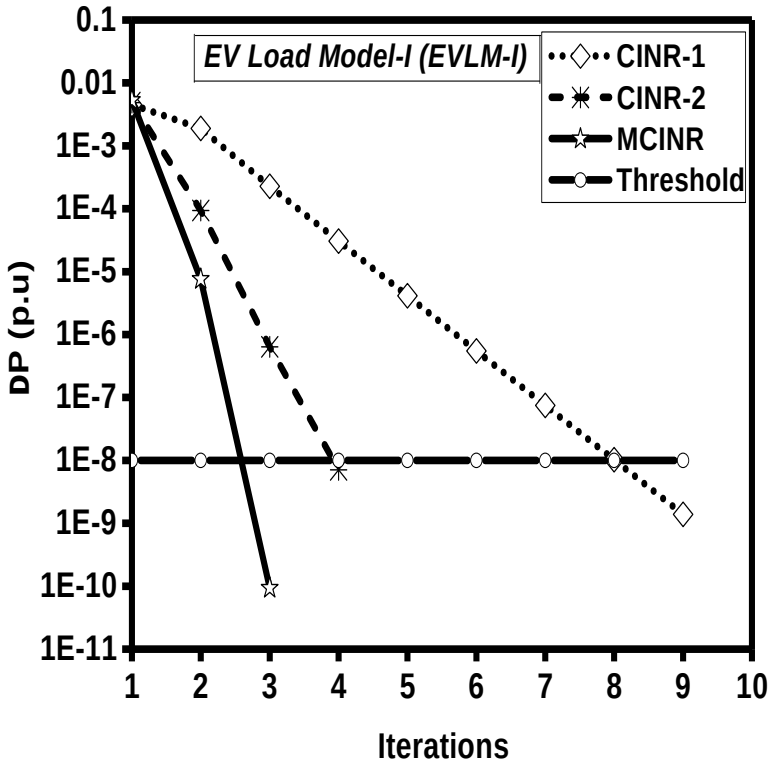

Figure 3.4: Power mismatch $max(\Delta P)$ on each iteration for $EVLM$-I

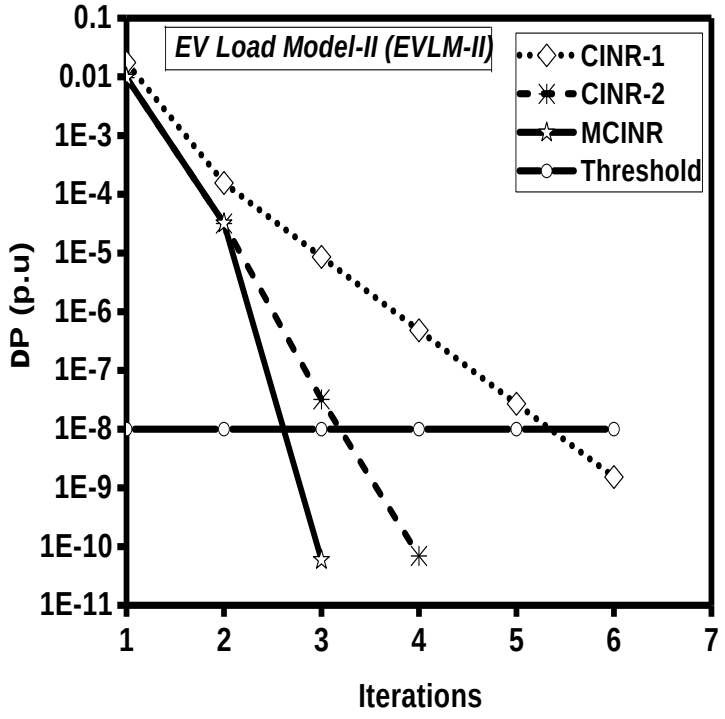

Figure 3.5: Power mismatch $max(\Delta P)$ on each iteration for $EVLM\text{-}II$

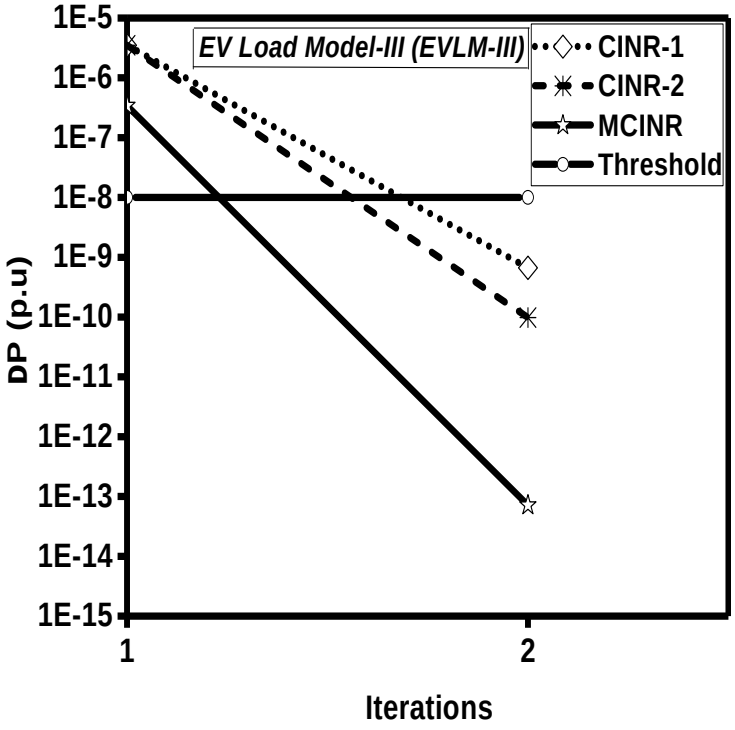

Figure 3.6: Power mismatch $max(\Delta P)$ on each iteration for $EVLM\text{-}III$

The proposed algorithm ($MCINR$) is tested on radial and meshed systems and the results obtained are compared with existing current injection based algorithms. The robustness of the method is tested by varying the system loading and R/X ratios of the systems. The effectiveness of the proposed algorithm, $MCINR$, is compared with existing methods viz. conventional Newton-Raphson power flow (CNR), $CINR-I$ and $CINR-II$ in terms of convergence characteristics, loading variation and R/X ratio variation. Test systems adopted for the analysis are detailed in Table. 3.3.

Table 3.3: Description of test systems

Unbalanced Radial System			Meshed System		
Total Buses	No. of PV Buses	No. of PQ Buses	Total Buses	No. of PV Buses	No. of PQ Buses
18	3	14	24	10	13
84	9	74	118	53	64
140	15	124	300	68	231

Convergence characteristics for unbalance radial systems

Variation of maximum power mismatch, $max(\Delta P)$, for $CINR-I$, $CINR-II$, and $MCINR$ with respect to iterations has been plotted in Figs. 3.7, 3.8 and 3.9 for unbalanced radial test systems viz. 18-, 84- and 140-buses respectively. It is observed that the convergence property in terms of maximum power mismatch is better in case of the proposed algorithm, ($MCINR$), as compared to $CINR-I$ and $CINR-II$. Thus, for the proposed algorithm, ($MCINR$), the convergence rate is faster and requires less number of iterations as compared to $CINR-I$ and $CINR-II$. The required computational time is to converge on steady state value of power flow solution is shown in Table 3.4. It is observed that required computational time is lower in case of ($MCINR$) as compared to $CINR-I$ and $CINR-II$.

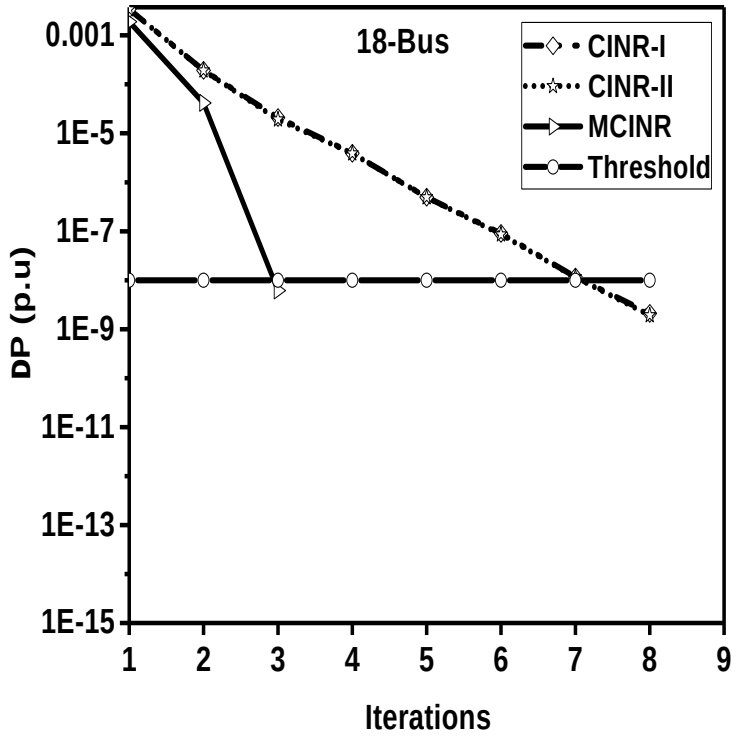

Figure 3.7: Power mismatch $max(\Delta P)$ on each iteration for 18-Bus test systems

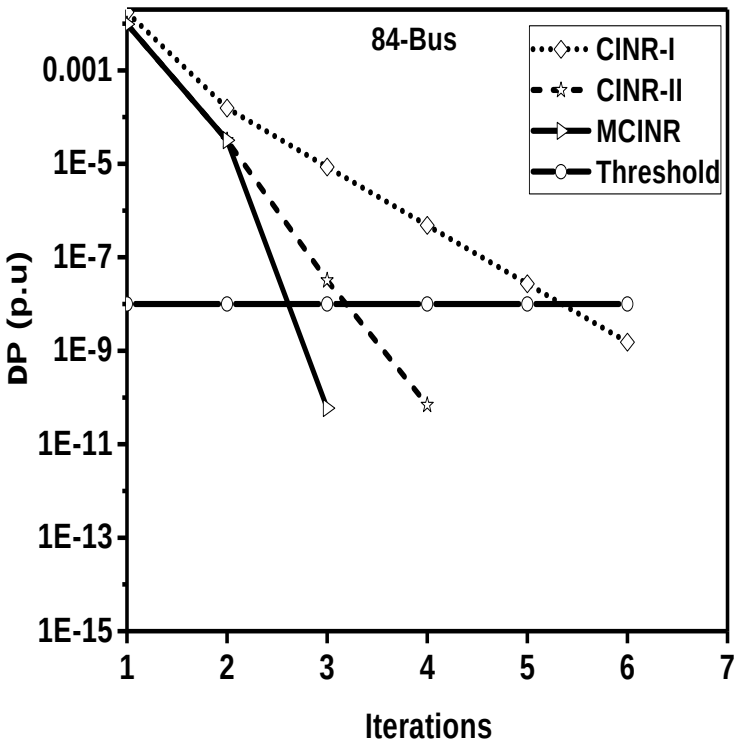

Figure 3.8: Power mismatch $max(\Delta P)$ on each iteration for 84-Bus test systems

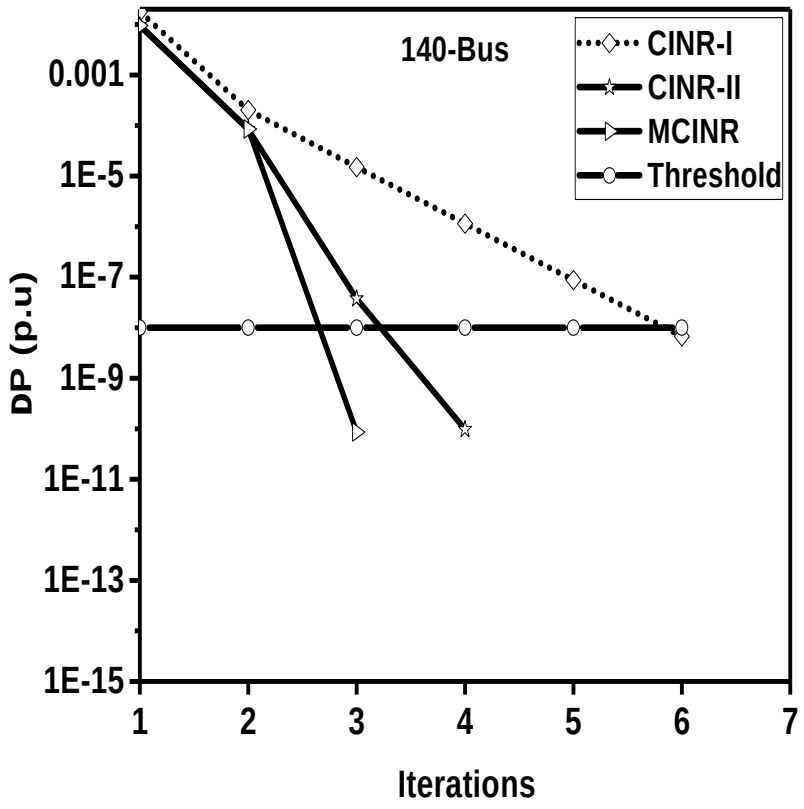

Figure 3.9: Power mismatch $max(\Delta P)$ on each iteration for 140-Bus test systems

Table 3.4: Required computational time for meshed system

Test System	$CINR-I$	$CINR-II$	$MCINR$
18	0.0083	0.0092	0.0043
84	0.0093	0.0071	0.0066
140	0.0121	0.0082	0.0072

Convergence characteristics for meshed systems

The maximum power mismatches, $max(\Delta P)$, for $CINR-I$, $CINR-II$, CNR and $MCINR$ with respect to iterations has been plotted in Figs. 3.10, 3.11 and 3.12 for meshed test systems viz. 24-, 118- and 300-buses respectively. It can be observed that the convergence characteristic in terms of maximum power mismatch value of $MCINR$ is better as compared to CNR, $CINR-I$, and $CINR-II$. In $MCINR$, the convergence rate is faster, and the required number of iterations is also lesser as compared to CNR,

$CINR-I$, and $CINR-II$. The required computational time is to converge on steady state value of power flow solution is shown in Table 3.5. It is observed that required computational time is lower in case of ($MCINR$) as compared to $CINR-I$,$CINR-II$ and CNR. In the case of CNR methods, the required CPU time is high if the number of buses is large for the proposed method, computation time remains relatively lower with the increasing number of buses. Hence, it can be concluded that required computational time for matrix update and inversion are better than CNR technique.

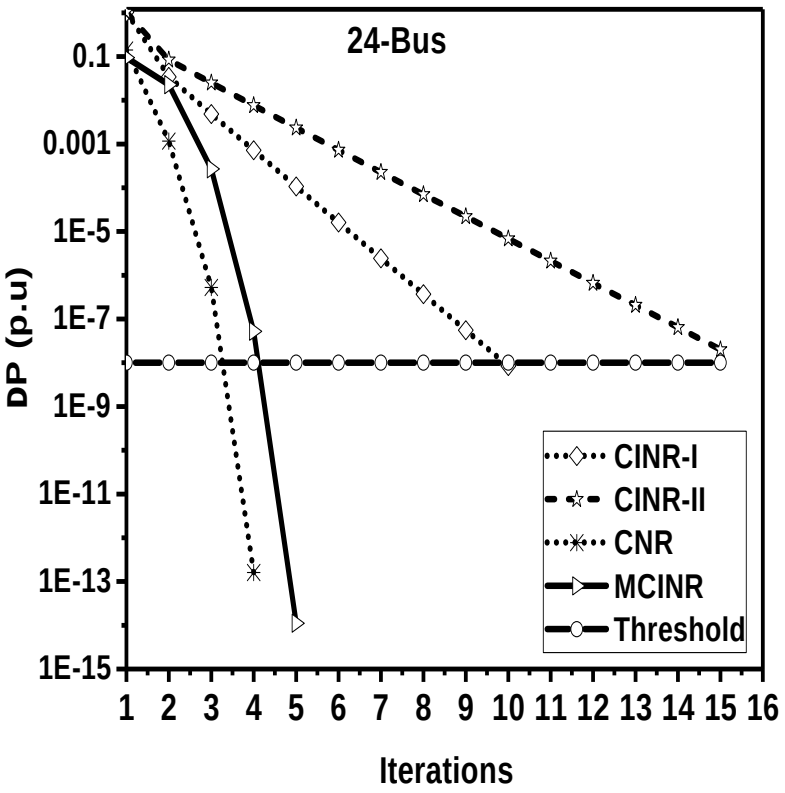

Figure 3.10: Power mismatch $max(\Delta P)$ on each iteration for 24-Bus test systems

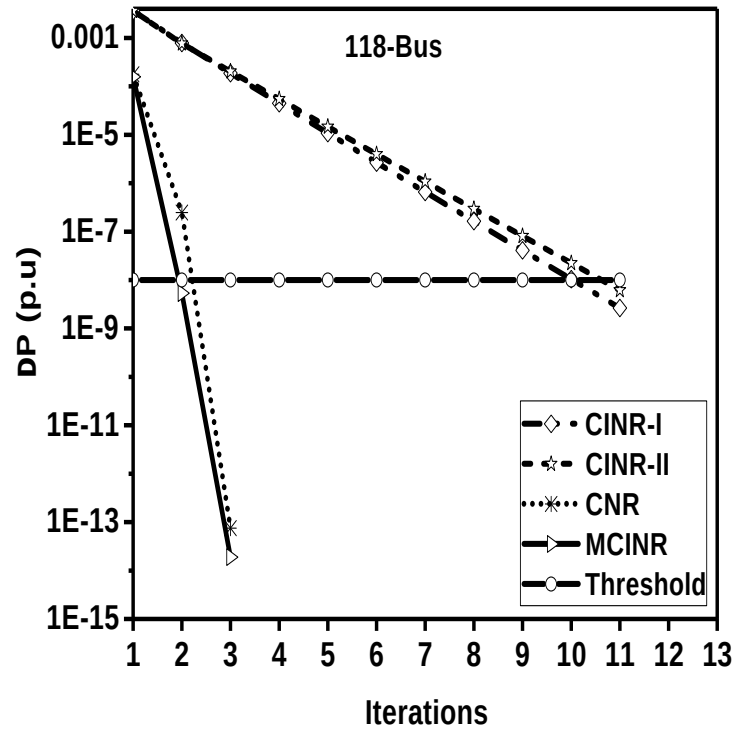

Figure 3.11: Power mismatch $max(\Delta P)$ on each iteration for 118-Bus test systems

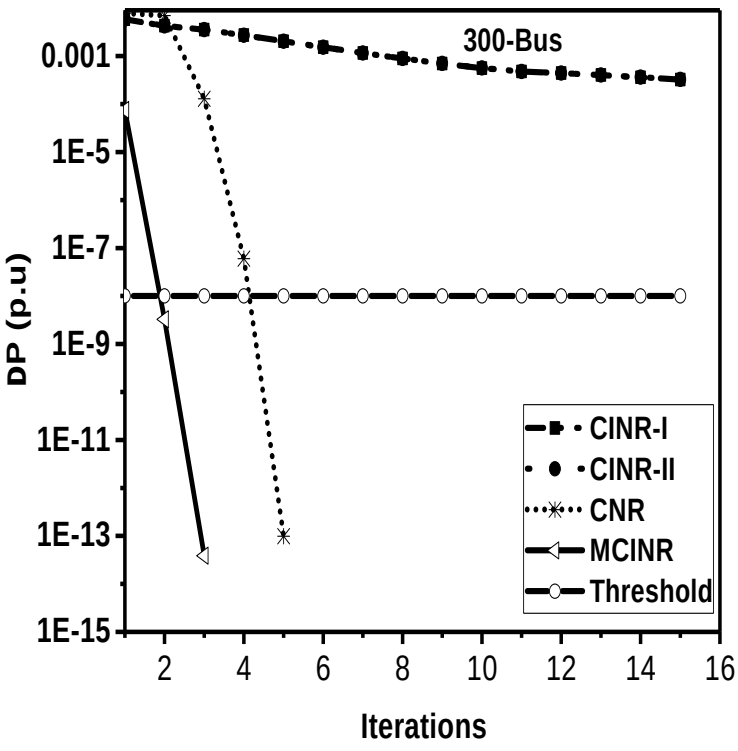

Figure 3.12: Power mismatch $max(\Delta P)$ on each iteration for 300-Bus test systems

Table 3.5: Required computational time for meshed system

Test System	CINR-I	CINR-II	CNR	MCINR
24	0.00604	0.00924	0.0179	0.00416
118	0.01253	0.01693	0.4902	0.00519
300	0.03541	0.04138	0.983	0.00984

Loading factor characteristics for unbalanced radial systems

The performance of power flow algorithm is highly dependent on the loading scenario of a system. It is also important to study the robustness of the proposed algorithm for different loading conditions. In this study, the loads on the test systems are increased without increasing the generation at PV buses. Then, all the algorithms ($CINR-I$, $CINR-II$, and $MCINR$) are applied to solve the power flow of these test systems (with increased loads). The robustness of the proposed algorithm ($MCINR$) concerning different loading conditions for the radial system are discussed as follows.

The loading factor is gradually increased up to its maximum point of convergence of load flow achieved, and the outcomes for algorithms are presented in Figs. 3.13, 3.14 and 3.15. It is observed that the handling of the loading factor is better for the proposed algorithm ($MCINR$) as compared to $CINR-I$ and $CINR-II$. As the loading factor increases, the performance of both, $CINR-I$ and $CINR-II$, starts deteriorating but the performance of the proposed method ($MCINR$) turns out to be quite robust in terms of convergence at higher possible loading.

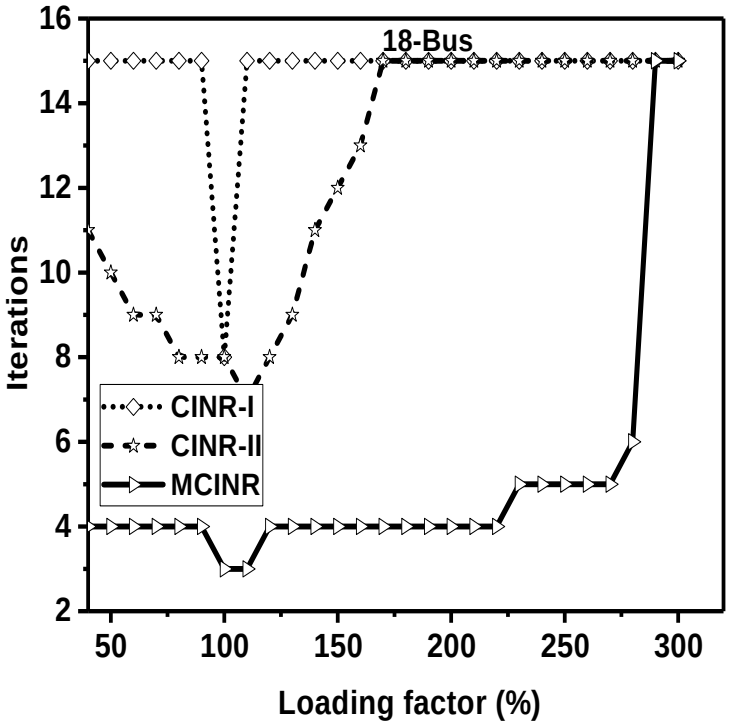

Figure 3.13: Loading factor vs iteration for 18-Bus test system.

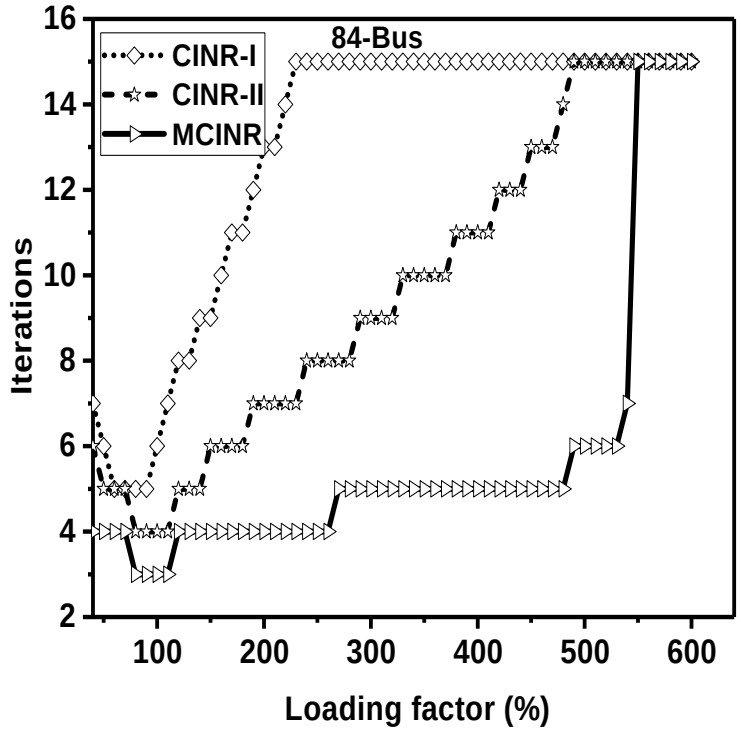

Figure 3.14: Loading factor vs iteration for 84-Bus test system.

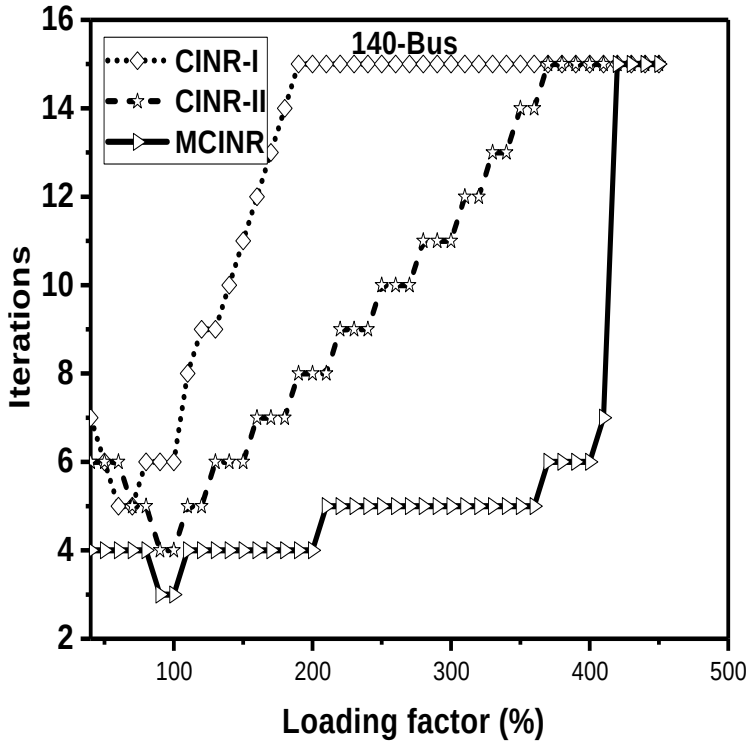

Figure 3.15: Loading factor vs iteration for 140-Bus test system.

Loading factor characteristics for meshed systems

The robustness of the proposed algorithm for increased loading conditions of the meshed systems viz. 24-, 118-bus and 300-bus are demonstrated in Figs. 3.16, 3.17 and 3.18. It is observed that for high loading factor, proposed method ($MCINR$) performs better than the $CINR-I$ and $CINR-II$ and performance of the ($MCINR$) is almost equal or slightly better than CNR.

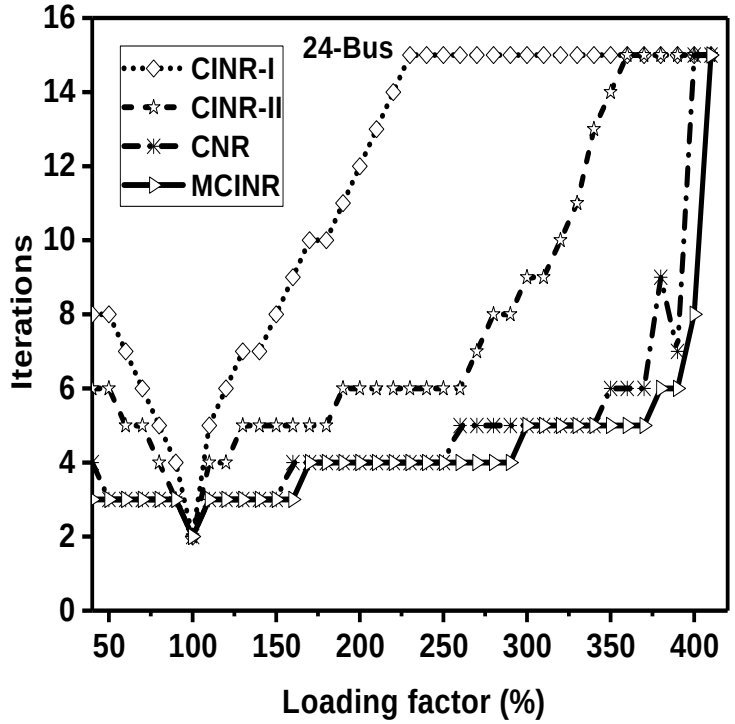

Figure 3.16: Loading factor vs iteration for 24-Bus system.

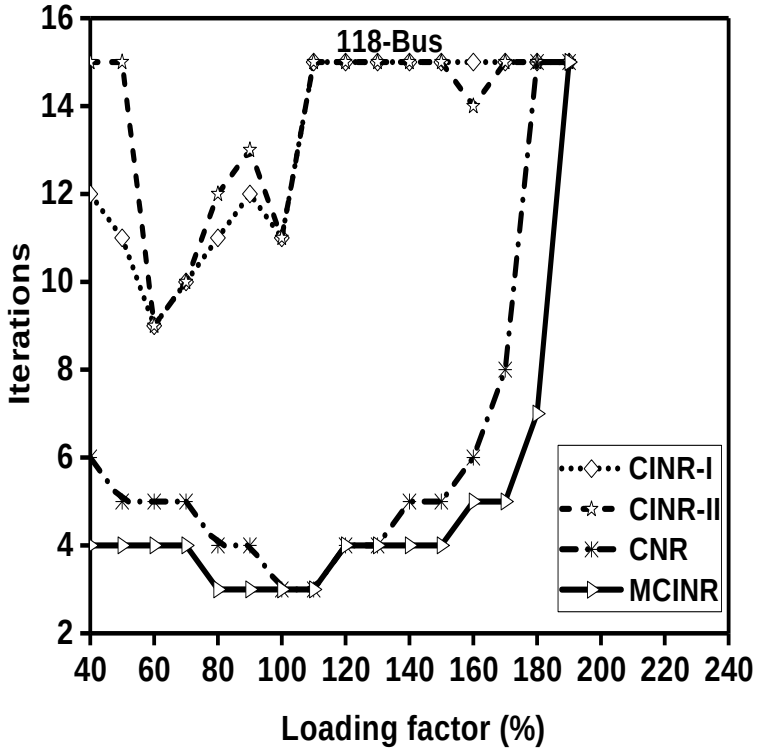

Figure 3.17: Loading factor vs iteration for 118-Bus system.

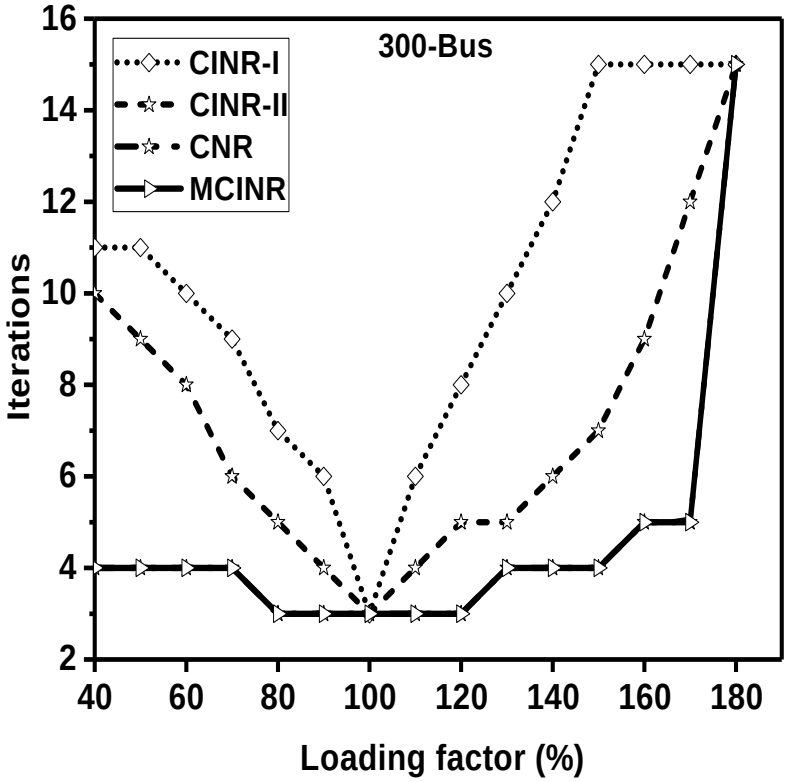

Figure 3.18: Loading factor vs iteration for 300-Bus system.

R/X Ratio characteristics for unbalanced radial systems

Electrical power distribution systems have normally very high R/X ratios as compared to the transmission system. The R/X ratios are used to test the robustness against R/X ratios of the power flow algorithm. The R/X ratios (%) was increased to see the proposed algorithm can work satisfactorily without failing. For example, when R/X ratio is considered as 300%, this means that value of R is 3 times the value of X. In this subsection, the robustness of the proposed algorithm is examined for the unbalanced radial system with higher R/X ratios.

The performance of different current injection-based algorithms with gradually increased R/X ratios for radial systems are shown in Figs. 3.19, 3.20 and 3.21. It can be observed that the performance of $CINR-I$ and $CINR-II$ depreciates with the increase in R/X ratios for radial systems. The performance of the proposed method ($MCINR$) is better in case of the radial systems as compared to other existing methods.

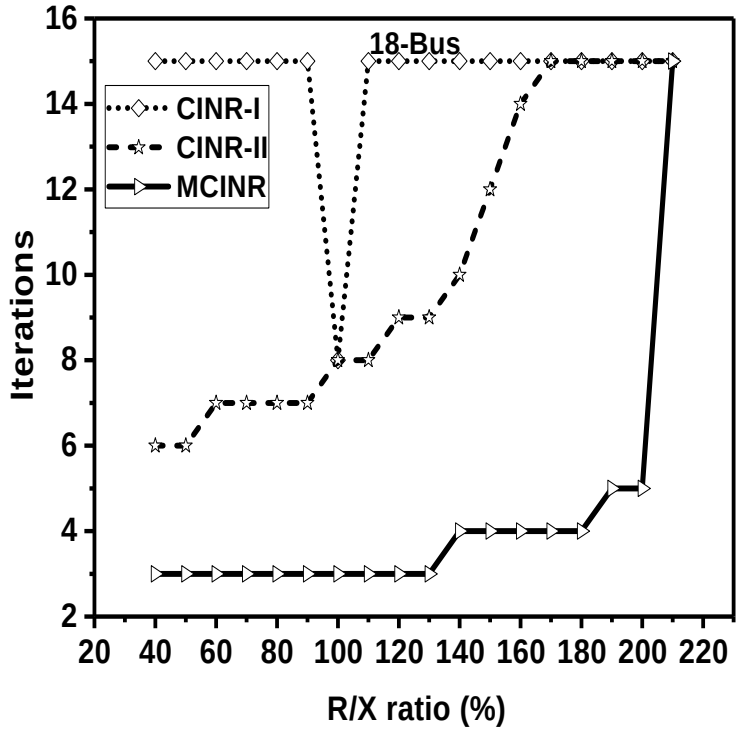

Figure 3.19: R/X ratio vs iteration for 18-Bus test system.

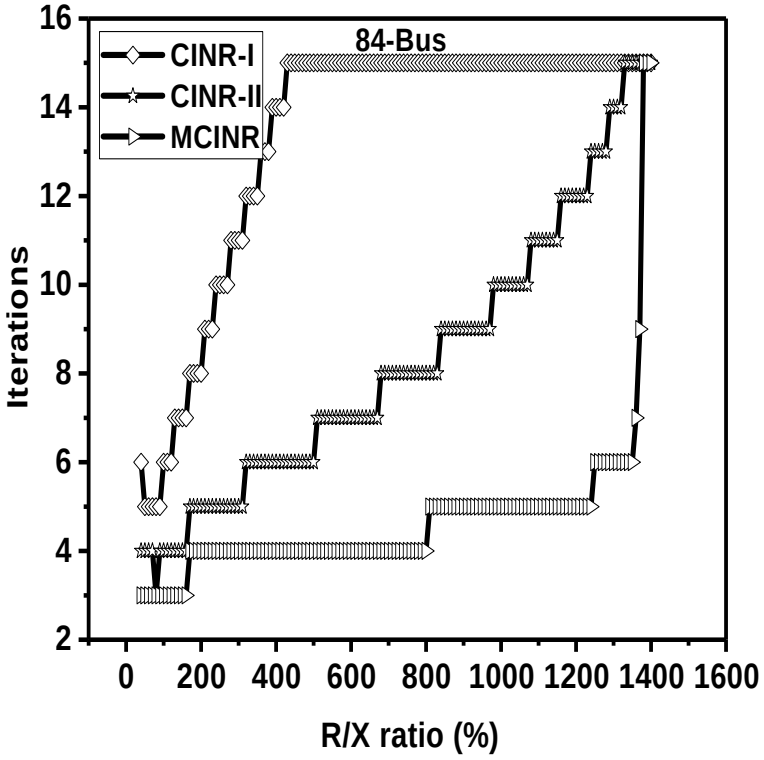

Figure 3.20: R/X ratio vs iteration for 84-Bus test system.

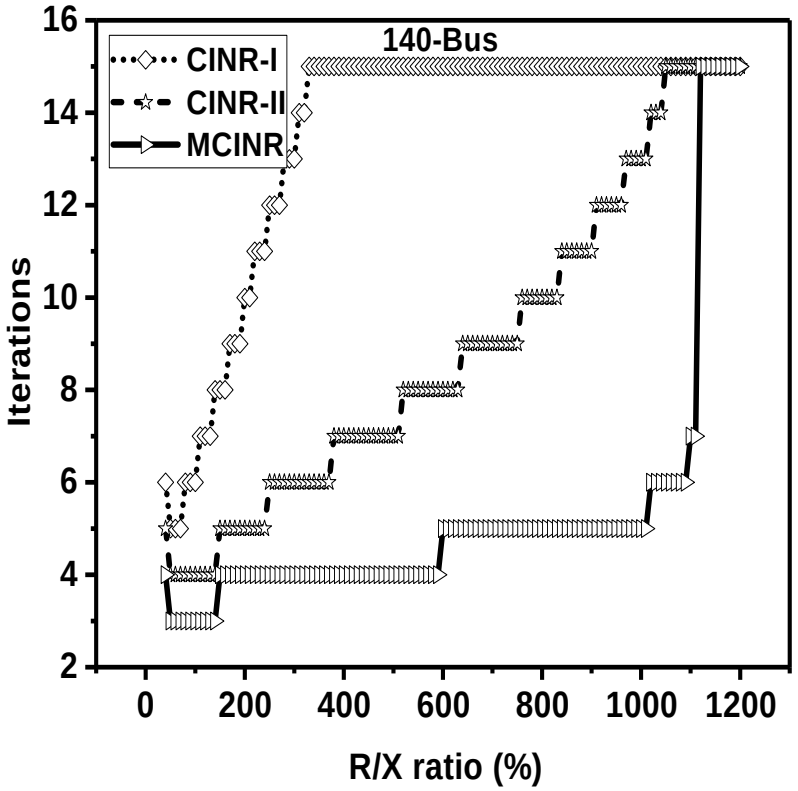

Figure 3.21: R/X ratio vs iteration for 140-Bus test system.

R/X Ratio characteristics for meshed system

The performance of different current injection-based algorithms with gradually increasing R/X ratios for meshed systems is shown in Figs. 3.22, 3.23 and 3.24. It can be observed that the performance of $CINR-I$ and $CINR-II$ deteriorates with the increasing R/X ratios for meshed systems. The performance of the proposed method ($MCINR$) is better in case of the meshed system as compare to other existing methods. It can be said that this algorithm can effectively solve the meshed system having a large number of PV buses as well as radial systems with PV bus.

Also, the robustness and efficiency of the proposed method for both meshed and radial system are better than the other current injection-based methods and almost similar to CNR method in case of the meshed system.

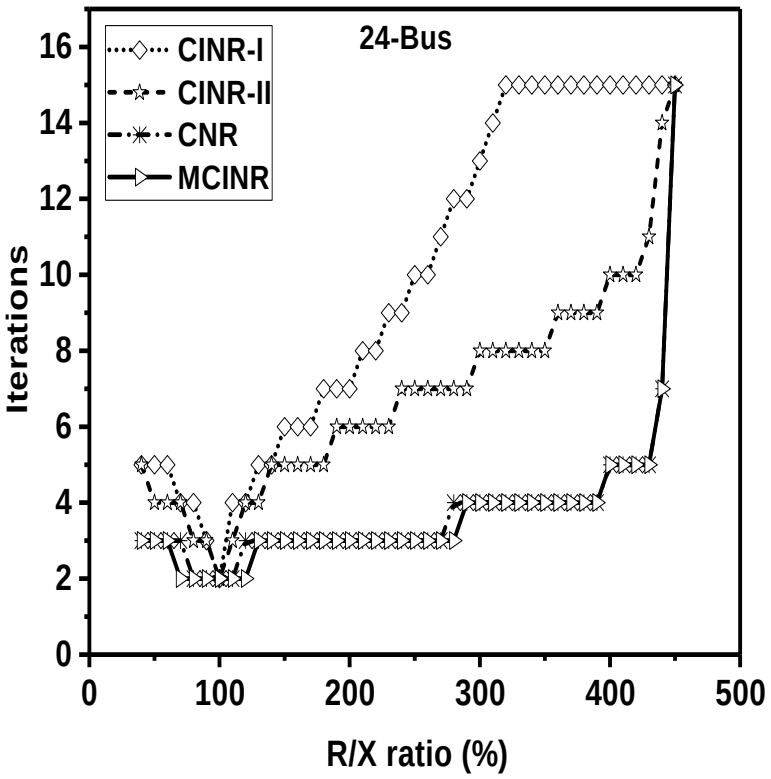

Figure 3.22: R/X ratio vs iteration for 24-Bus system.

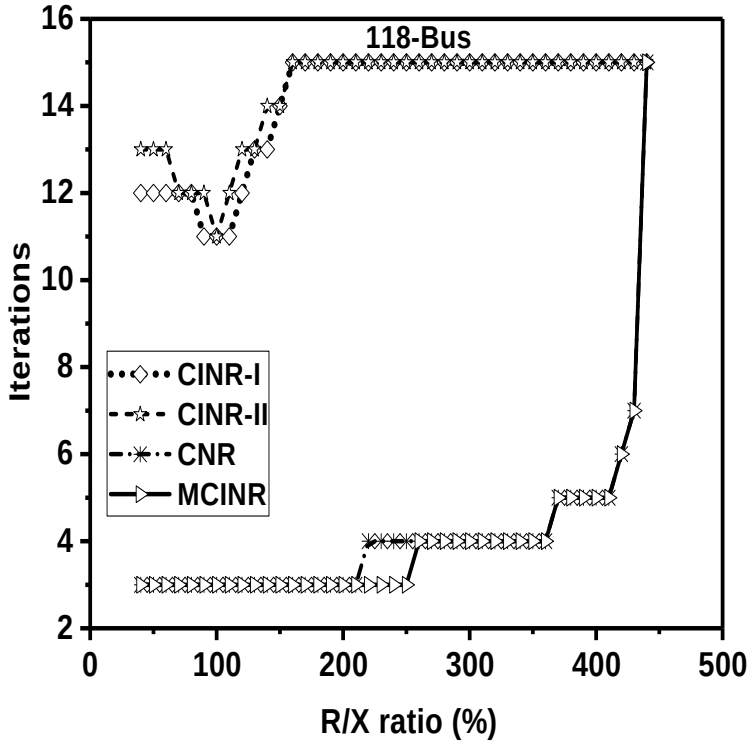

Figure 3.23: R/X ratio vs iteration for 118-Bus system.

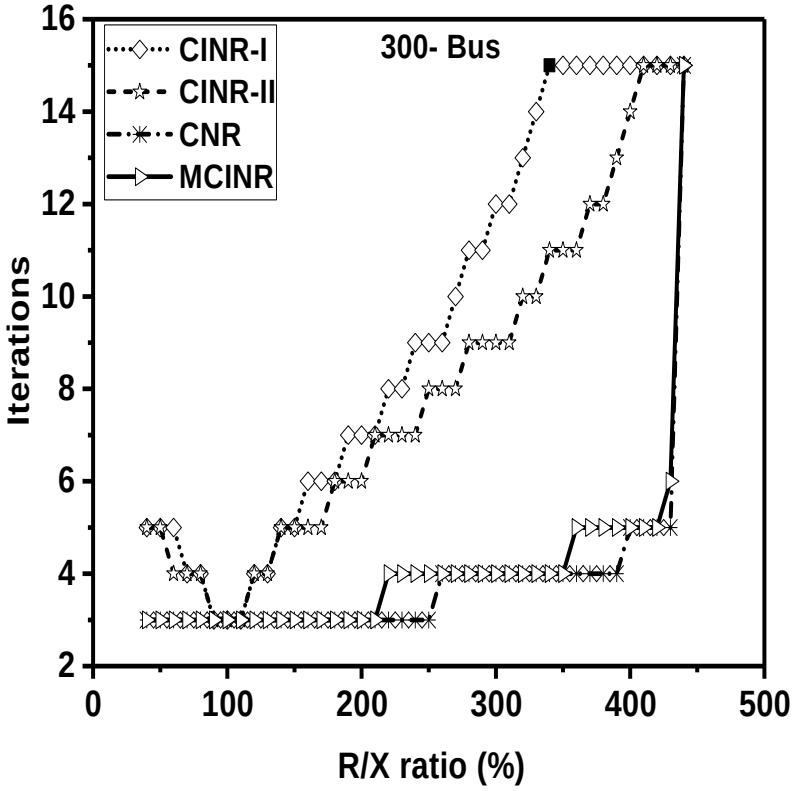

Figure 3.24: R/X ratio vs iteration for 300-Bus system.

3.4.4 Impact of EV load models on load flow

In order to analyse the effect of the EV load models on the distribution system, real and reactive power losses indices (ILP & ILQ), voltage profile index (IVD) and MVA capacity index (IC) are evaluated in this section. To show the effectiveness of PHEVs load inclusion in the load flow studies, a further separate study with 35%, 54% and 62% penetration level of vehicles are performed. The step-by-step procedure of modified current injection Newton-Raphson ($MCINR$) based load flow algorithm is shown in Algorithm 1. The candidate buses for DGs integration can be obtained by finding the maximum value of loss saving in the distribution system. The bus which has maximum loss saving value is chosen as the best location to allocate the DGs. The optimal locations and scheduled DGs power for all the load models are bus number 2, 5, 28, 8, 15, 27, 3, 14, 29 and 30 along with the DG's (indexed in alphabetical order) is presented in Fig. 3.25. The active power losses with and without DGs are depicted in Table. 3.6. It can be observed from

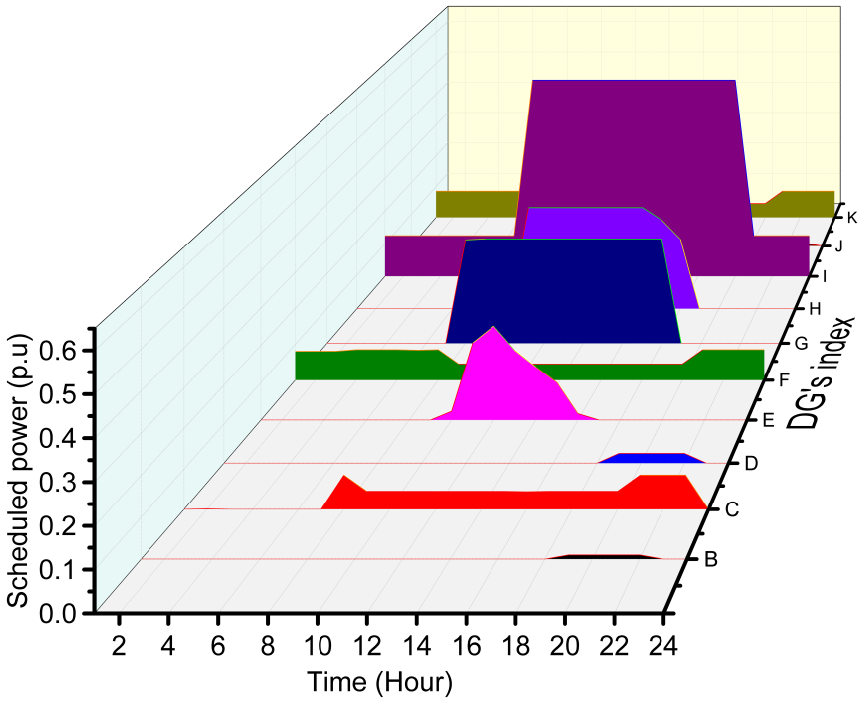

Figure 3.25: Scheduled DGs power

the Table. 3.6 that the active power losses are significantly reduced in the presence of DGs for all the EV load models. The maximum of 32.593% loss shaving is observed for $EVLM\text{-}II$ at 62% penetration of vehicles. At this point, it is also important to note that the active power loss in the case of $EVLM\text{-}II$ is higher in comparison to the $EVLM\text{-}I$ & $EVLM\text{-}III$. To compare the effect of EV load models in $MCINR$ load flow formulation,

Table 3.6: Active power loss with and without DGs

Penetration	With DGs			Without DGs		
	$EVLM\text{-}I$	$EVLM\text{-}II$	$EVLM\text{-}III$	$EVLM\text{-}I$	$EVLM\text{-}II$	$EVLM\text{-}III$
35%	2.9559	2.991	2.9587	4.3161	4.2228	4.3921
54%	2.9521	2.9857	2.9553	4.3744	4.4134	4.378
62%	2.9484	2.9738	2.9502	4.3725	4.4117	4.3765

three indices are defined: (i) Real and Reactive power losses indices (ILP & ILQ) (ii) Voltage profile index (IVD) and (iii) MVA Capacity index (IC).

Figs. 3.26, 3.27 and 3.28 shows the hourly ILP of distribution system for various penetration levels of EVs for $EVLM\text{-}I$, $EVLM\text{-}II$ and $EVLM\text{-}III$. It can be observed

that real power loss index with load model $EVLM\text{-}II$ is higher as compared to the polynomial type load model $EVLM\text{-}I$, and constant current load model $EVLM\text{-}III$ at each penetration level of vehicles. These observation are directly related to real power losses in distribution system and it is mentioned earlier in Table. 3.6.

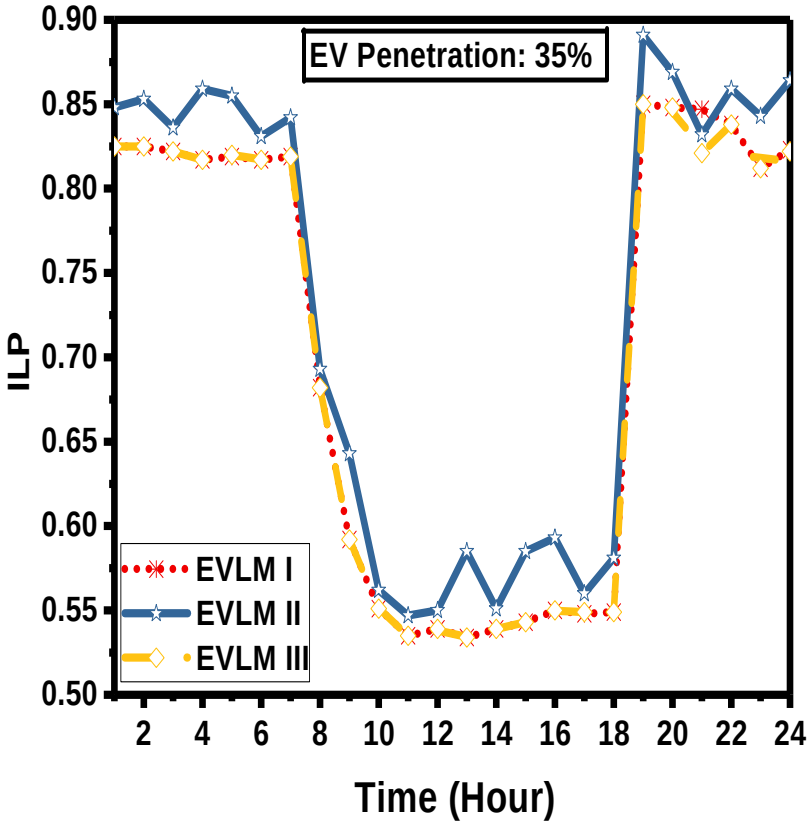

Figure 3.26: Hourly ILP at 35% penetration level of EVs

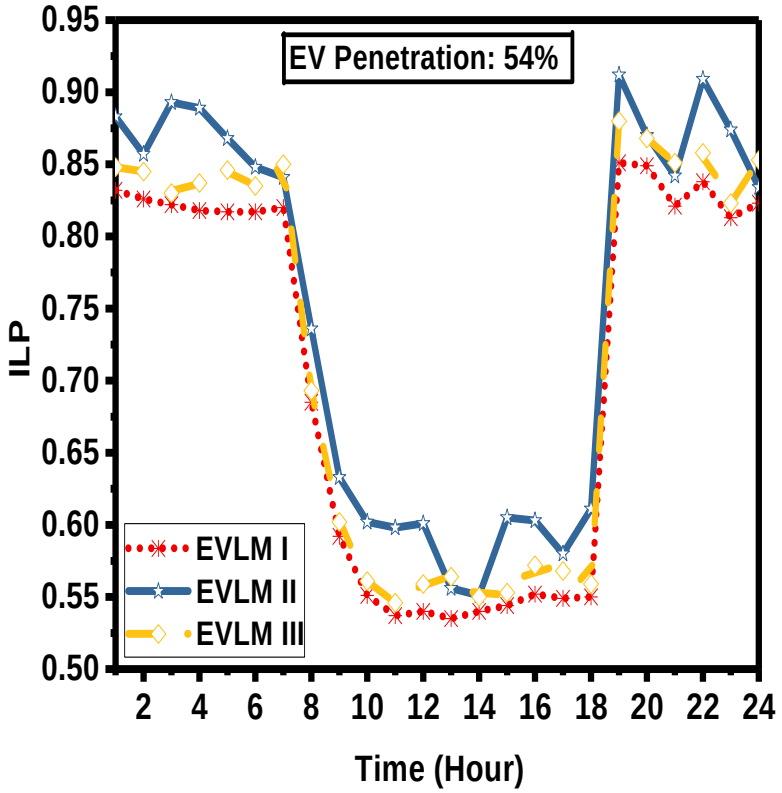

Figure 3.27: Hourly ILP at 54% penetration level of EVs

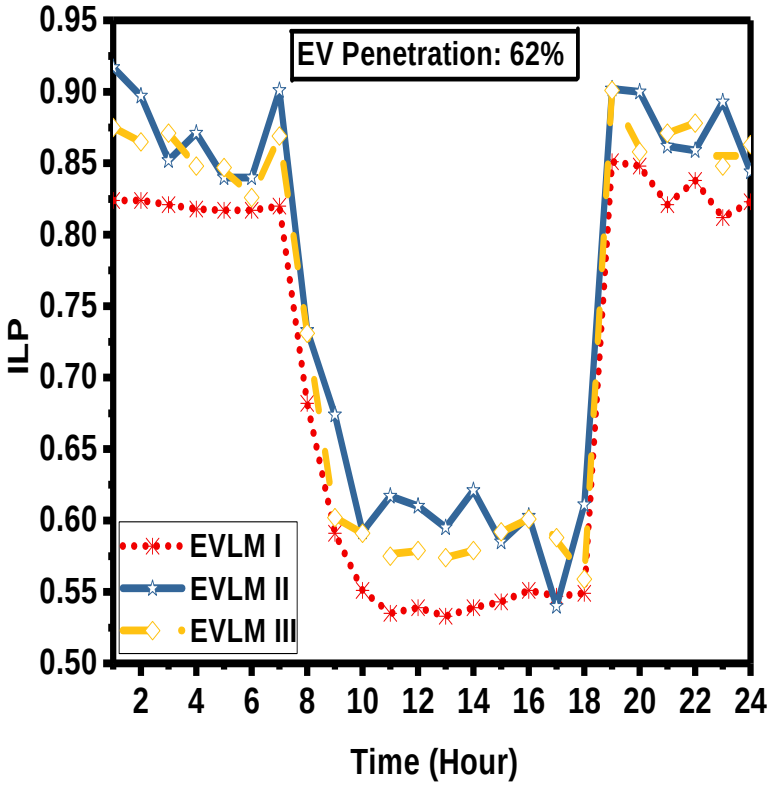

Figure 3.28: Hourly ILP at 62% penetration level of EVs

Figs. 3.29, 3.30 and 3.31 shows the hourly reactive power loss index (ILQ) of distribution system for $EVLM\text{-}I$, $EVLM\text{-}II$ and $EVLM\text{-}III$ at 35%, 54% and 62% penetration levels of EVs respectively. It can be observed that reactive power loss index with load model $EVLM\text{-}II$ is higher in comparison to polynomial type load model $EVLM\text{-}I$ and constant current load model ($EVLM\text{-}III$) at each penetration level.

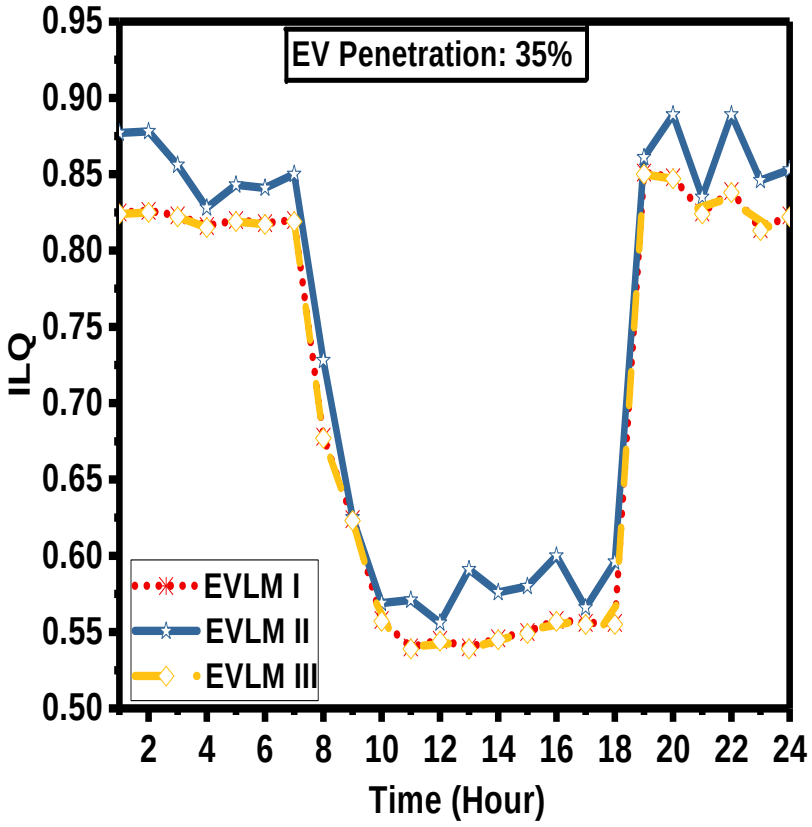

Figure 3.29: Hourly ILQ at 35% penetration level of EVs

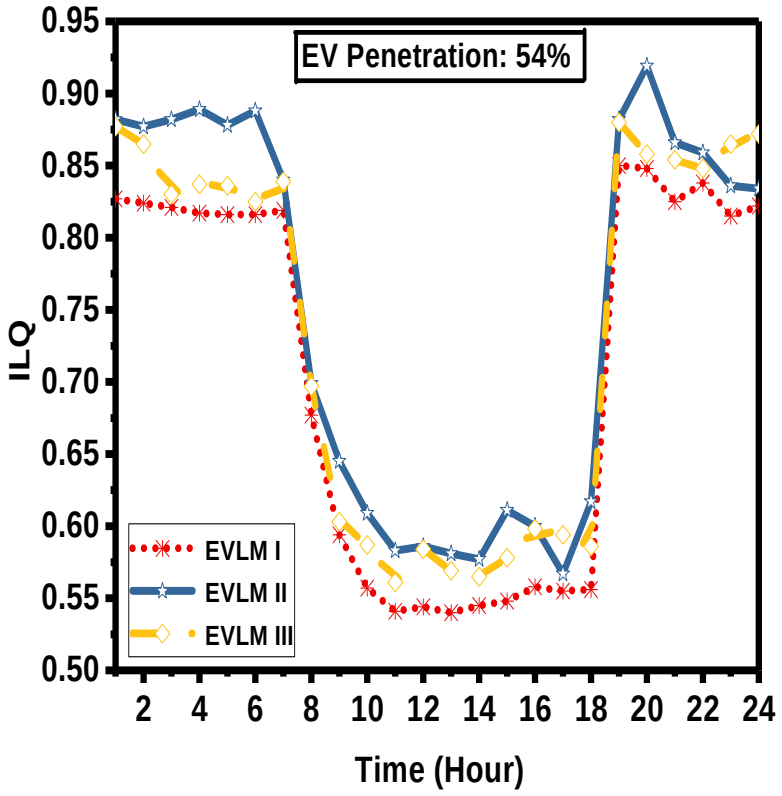

Figure 3.30: Hourly ILQ at 54% penetration level of EVs

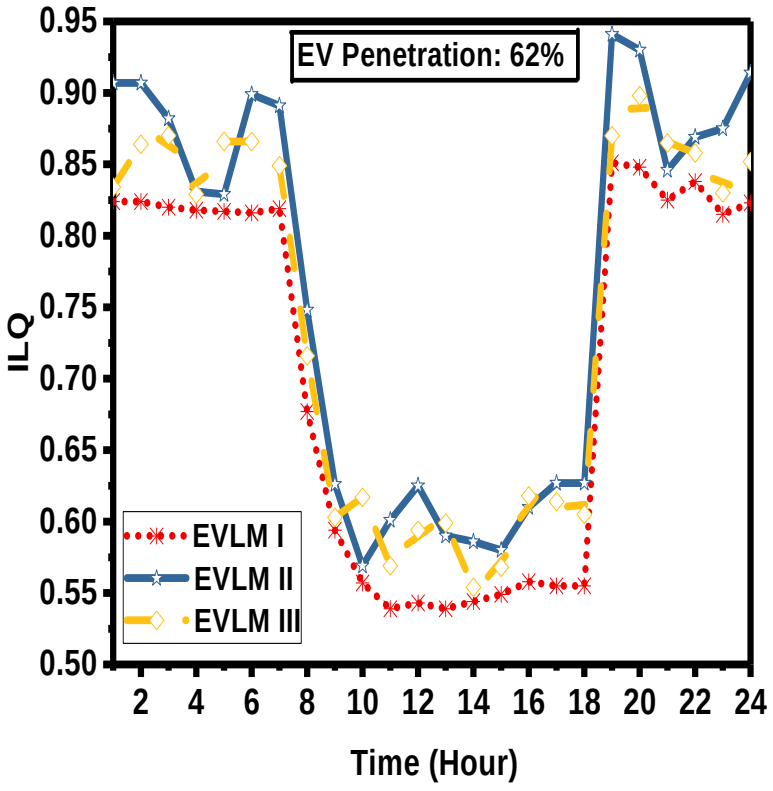

Figure 3.31: Hourly ILQ at 62% penetration level of EVs

The behavior of voltage profile index (IVD) directly refers to power quality related issues. Fig. 3.32 shows the voltage profile index (IVD) of distribution system for EVs load models $EVLM\text{-}I$, $EVLM\text{-}II$ and $EVLM\text{-}III$ at 35%, 54% and 62% penetration levels of vehicles. From Fig. 3.32, higher value of IVD is observed for load model $EVLM\text{-}II$ in comparison to the load models $EVLM\text{-}I$ and $EVLM\text{-}III$. Similar trend is observed at all the penetration levels of electric vehicles.

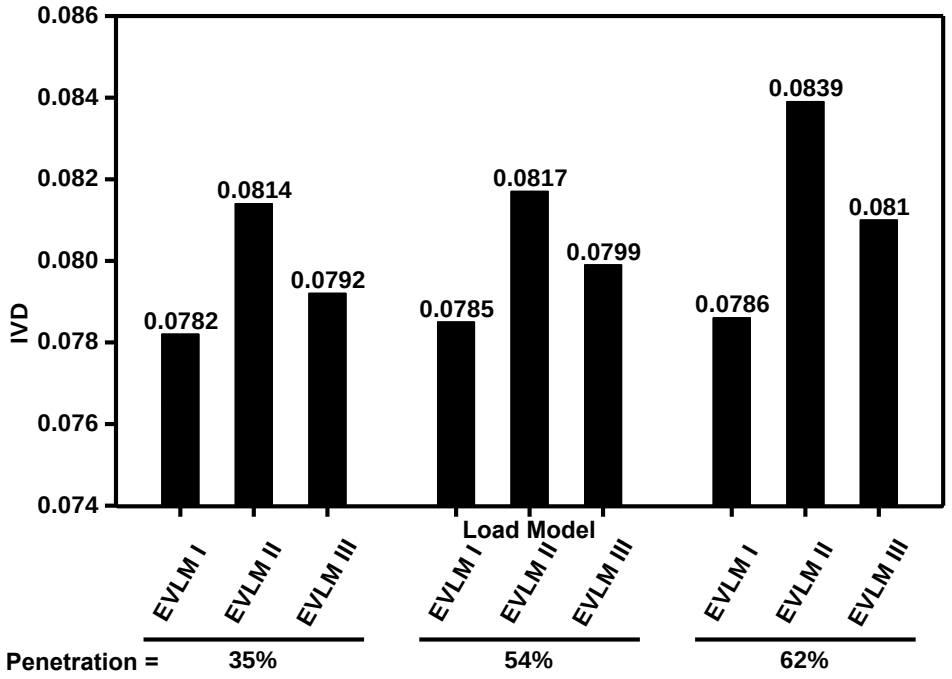

Figure 3.32: Voltage profile index at different penetration level of EVs

The MVA capacity index (IC) provides the information regarding the utilized line MVA capacity of the distribution system. The values of ICs for $EVLM\text{-}I$, $EVLM\text{-}II$ and $EVLM\text{-}III$ at 35%, 54% and 62% penetration levels of vehicles are depicted in Fig. 3.33. From Fig. 3.33, it is observed that for the utlized MVA capacity of the line, the voltage dependent load model $EVLM\text{-}II$ is higher. In addition, it is also observed that MVA capacity index increases as the penetration levels of electric vehicles increases on the distribution system.

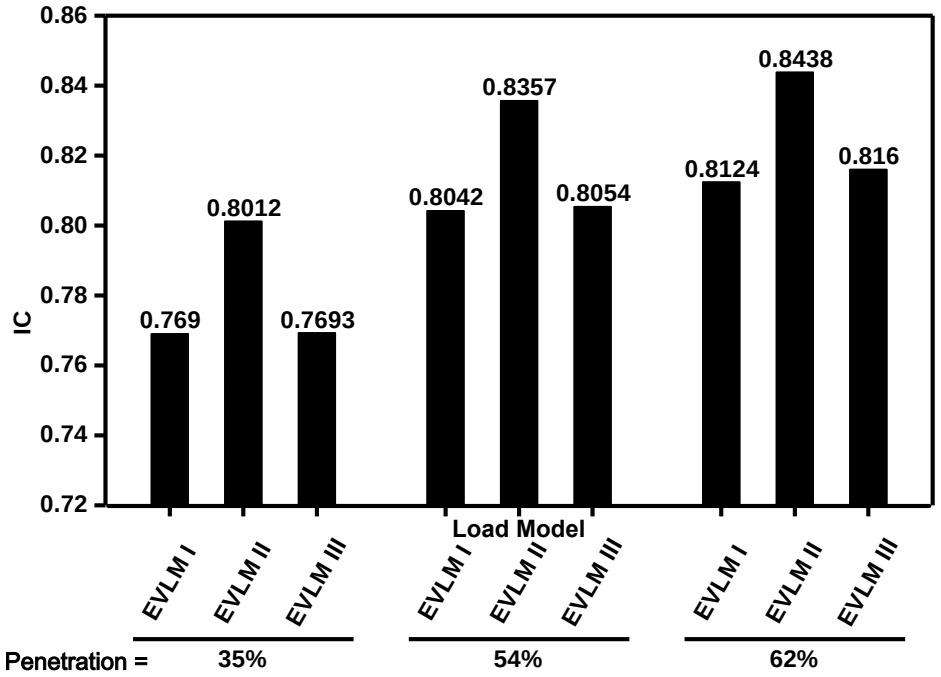

Figure 3.33: MVA capacity index at different penetration level of EVs

3.5 Summary

A modified current injection Newton-Raphson ($MCINR$) based load flow method incorporating three different types of EV load models viz. polynomial type load model $EVLM\text{-}I$, voltage dependent load model $EVLM\text{-}II$ and constant current load model $EVLM\text{-}III$ is proposed. The modified power flow method ($MCINR$) with these three load models of EVs are implemented on 38-bus distribution system to investigate the effects of EV load modelling on load flow methods for three penetration level of EVs. Moreover, it is also observed that proposed modification in power flow formulation enhances the performance and efficiency, without compromising the robustness. To analyze the outcome of the proposed method, three performance indices viz. (i) real and reactive power losses indices (ILP & ILQ), (ii) voltage profile index (IVD) and (iii) MVA capacity index (IC) are evaluated. The absolute values of indices (ILP, ILQ, IVD and IC) show a quantitative indication of the effectiveness of including of EV load models in the proposed modified current injection Newton-Raphson ($MCINR$) based load flow algorithm for distribution system.